Digital landscapes of deglaciation: Identifying Late Quaternary glacial lake outburst floods using LiDAR

[1]Thorndycraft, V.R., [2]Cripps, J.E. and [1]Eades, G.

[1]Department of Geography, Royal Holloway University of London, Egham, Surrey, UK. TW20 0EX. Email: Varyl.Thorndycraft@royalholloway.ac.uk

[2]Department of Geography, Simon Fraser University, Burnaby, British Columbia, Canada.

Abstract: High resolution DEMs obtained from LiDAR topographic data have led to improved landform inventories (e.g. landslides and fault scarps) and understanding of geomorphic event frequency. Here we use airborne LiDAR mapping to investigate meltwater pathways associated with the Tweed Valley palaeo ice-stream (UK). In particular we focus on a gorge downstream of Palaeolake Milfield, previously mapped as a sub-glacial meltwater channel, where the identification of abandoned headcut channels, run-up bars, rock-cut terrace surfaces and eddy flow features attest to formation by a sub-aerial glacial lake outburst flood (GLOF) caused by breaching of a sediment dam, likely an esker ridge. Mapping of these landforms combined with analysis of the gorge rim elevations and cross-section variability revealed a two phase event with another breach site downstream following flow blockage by high relief drumlin topography. We estimate the magnitude of peak flow to be 1-3 x 10^3 m^3/s, duration of the event to range from 16-155 days, and a specific sediment yield of 10^7-10^9 $m^3/km^2/yr$. We identified other outburst pathways in the lower Tweed basin that help delineate an ice margin position of the retreating Tweed Valley ice stream. The results suggest that low magnitude outburst floods are under-represented in Quaternary geomorphological maps. We therefore recommend regional LiDAR mapping of meltwater pathways to identify other GLOFs in order to better quantify the pattern of freshwater and sediment fluxes from melting ice sheets to oceans. Despite the relatively low magnitude of the Till outburst event, it had a significant impact on the landscape development of the lower Tweed Valley through the creation of a new tributary pathway and triggering of rapid knickpoint retreat encouraging new regional models of post-glacial fluvial landscape response.

Keywords: LiDAR; Geomorphological Mapping; Glacial Lake Outburst Floods; Late Quaternary; Landscape evolution

Introduction

The availability of high resolution Digital Elevation Models (DEMs) has transformed investigations of earth surface processes and dynamics. According to Roering et al. (2013), LiDAR data have influenced geomorphology in three main ways: 1) by providing a detailed base map for subsequent field mapping and sample collection; 2) by facilitating rapid and accurate description of morphological patterns for model testing over wide spatial areas; and 3) by facilitating identification of unanticipated landforms. Since the availability of LiDAR technology and advances in data handling through Geographical Information Systems (GIS), the quantity and quality of published geomorphological maps have increased (Oguchi et al., 2011). The high spatial resolution of LiDAR data (0.25-2m) permits improved mapping that often results in discovery of previously unmapped landforms hidden beneath vegetation (e.g. Lin et al. 2013) or simply not discernible at lower spatial resolution

(Begg and Mouslopoulou, 2010). LiDAR has resulted in improved landslide inventories (e.g. Van Den Eeckhaut et al., 2011); the identification of landslide-dammed palaeolakes (Mackey et al., 2011); and recognition of small scale fault scarps (e.g. Begg and Mouslopoulou, 2010; Lin et al., 2013). It has also enabled improvements in the quantification and characterisation of landform elements, such as roughness and semi-variance to differentiate landslide morphological components (Glenn et al., 2006), and slope curvature for landscape evolution models (e.g. Hurst et al., 2012; Roering et al., 2013). In floodplain environments LiDAR data has allowed greater quantification of fluvial dynamics and sediment budgets (e.g. Notebaert et al., 2009), and improved mapping of sediment-landforms associated with alluvial geoarchaeology (Brown, 2008). Furthermore, LiDAR has been used in research covering a range of temporal scales, from long-term landscape evolution models (Hurst et al., 2012; Roering et al., 2013) and identification of Late Quaternary landforms (Van Den Eeckhaut et al., 2010; Mackey et al., 2011) to the scale of decadal landform response or single events (e.g. Notebaert et al, 2009; Cloke et al., 2013). In this paper we explore the potential of LiDAR for investigating the timescales of landscape change in Late Quaternary deglacial environments by testing whether high resolution DEMs can be used to decipher geologically near-instantaneous glacial lake outburst floods (GLOFs) from longer-term (decadal to centennial) meltwater processes.

The historic trend of glacier and ice sheet shrinkage (e.g. Helm et al., 2014), is predicted to continue in response to future climate change (IPCC, 2013). This has led to growing concern regarding the hazard implications of GLOFs from ice and moraine dammed lakes, increasing in size and number (e.g. Carrivick and Quincey, 2014), created by ice recession particularly in mountainous regions (e.g. Kattelmann, 2003; McKillop and Clague, 2007a, 2007b; Korup and Tweed, 2007; Dussaillant et al., 2010). There is also uncertainty regarding the magnitude and rate of meltwater transfer from glaciers to the ocean (Carrivick and Tweed, 2013). Geomorphic evidence of palaeo-GLOFs can improve our understanding of the likely frequency, timing and impact of such events in the future. To date the main focus of Quaternary GLOF research has been at the megaflood scale (> 10^6 m^3s^{-1}), in particular from the North American ice sheets e.g. glacial lakes Missoula (e.g. Baker, 2009) and Agassiz (Teller et al., 2002; Murton et al., 2010; Clarke et al., 2003; 2004); and in Eurasia e.g. Lake Vitim (Margold et al., 2011) and the Altai region of Siberia (Baker et al., 1993; Carling et al. 2010). The reconstructed discharges of these megafloods can attain magnitudes in the order of 1 $x10^7$ m^3s^{-1} (Benito and O'Connor, 2003; Denlinger and O'Connell, 2010; Alho, et al., 2010). However, these exceptionally large events are unsuitable analogues for relatively low magnitude floods (that we define as events with peak flows < 10^5 m^3s^{-1}) associated with contemporary ice marginal lakes (Anacona et al., 2015).

Studies of modern GLOFs demonstrate that relatively low magnitude floods can result in distinct flood sedimentology, such as imbricated boulders, coarse channel gravels, expansion bars and finer sediment deposited at high elevations (e.g. Kershaw et al., 2005; Dusaillant et al., 2010). This implies that low magnitude Quaternary outbursts may be positively identified from geomorphic evidence, such as the Late Pleistocene Lake Wisconsin flood (1.5 x 10^5 m^3s^{-1}) reconstructed by Clayton and Knox (2008). However to date there is relative paucity of these smaller events observed in the geologic record. This likely reflects a lack of investigation, poor preservation of geomorphic evidence, the smaller scale of diagnostic landforms, and/or insufficient spatial resolution of mapping. Just as LiDAR has enabled greater detection of previously unmapped fault scarps (Begg and Mouslopoulou, 2010) and landslides (Van Den Eeckhaut et al., 2010) it might reveal a greater number of Quaternary palaeo-GLOF events than is known at present.

The aim of this paper is to evaluate the use of high resolution LiDAR digital mapping for elucidating meltwater drainage processes in former ice-marginal landscapes. In particular we focus on deciphering geologically near-instantaneous GLOF events from longer-term meltwater drainage as this has potential implications for understanding rates of: freshwater and sediment flux to oceans, which could help improve predictions associated with contemporary melting ice sheets and fluvial landscape evolution in formerly glaciated regions. To achieve the main research aim, the following objectives were addressed: 1) identification of suitable meltwater pathways where instantaneous GLOF versus long-term meltwater drainage could be tested; 2) mapping the geomorphology of chosen meltwater pathways using LiDAR; and 3) fieldwork to verify desk-top interpretations derived from the LiDAR data.

Methodology

Field site selection

The mapping of the former British-Irish Ice Sheet presented in the BRITICE GIS database (Clarke et al., 2004) was used as the basis for exploring potential ice marginal field sites associated with the retreating ice sheet. Regions with contemporary bedrock river gorges draining former glacial lake basins were targeted, as these provide the potential for testable alternative hypotheses related to complex ice-marginal meltwater processes and environments (Marren, 2005). The River Till basin in NE England (Figure 1) was selected due to: a) the location of Palaeolake Milfield within the basin; b) the location of the bedrock-floored Till Gorge draining this palaeolake basin; c) extensive previous mapping (Gunn, 1895; Clapperton, 1971; Payton, 1980; Passmore et al., 2003); d) contrasting models of lake drainage and gorge formation (e.g. Clapperton, 1971 and Payton, 1980); e) a recent overview of paraglacial response in the basin drawing on new data (Passmore and Waddington, 2009); and f) availability of 1m and 2m LiDAR data.

Geomorphological mapping

1 m and 2 m LiDAR datasets, collected by Geomatics Ltd using Optech LiDAR systems with a vertical elevation accuracy of 0.05-0.15m, were used for geomorphological mapping of the Till valley (Figure 2). The available 1 m LiDAR data follow the main river valleys with a larger swath covered by the 2m LiDAR, hence the main Till gorge was mapped using the 1m dataset, combined with 2m LiDAR to extend spatial coverage (Figure 2). Maps were produced within ArcMap 10 GIS software using a range of standard visualisation techniques (Figure 3) following Smith (2011), including greyscale rasters (Figure 2), Triangular Irregular Networks (TINs) (Figures 3a and 3c); slope DTMs (Figure 3b), hillshade rasters (Figures 3e and 3f) with multiple azimuth (Smith and Clarke, 2005). Visualisations were overlain using transparent layers to represent multiple variables, such as slope and elevation (e.g. Lin et al., 2013) (Figure 3d). Following standard protocols in Smith (2011) rasters were saved in GeoTIFF format and mapped landforms as ESRI shapefiles.

Quantitative mapping was carried out within ArcGIS 10 and HEC-GeoRAS, the ArcGIS extension of the HEC-RAS flood model, which was used to extract topographic data for flood modelling (Hydrologic Engineering Center, 2011). The automatic *XS cut lines* tool of HEC-GeoRAS was used to rapidly extract regular interval cross-sections from the LiDAR data to obtain the long-profiles of the gorge bed and rim (10m intervals), and to quantify gorge cross-sectional area (50m intervals). Targeted cross-sections (Figure 2) were extracted by manually creating the XS cut lines layer in HEC-GeoRAS to compare and contrast the cross-sectional form of key sites within the gorge. To calculate volumes, clipped rasters were created by tracing targeted contour lines, based on geomorphological interpretation, and the volume beneath the selected contour level was calculated using the ArcGIS volume tool. The combined 1m and 2 LiDAR raster was used to estimate the volume of material eroded from the gorge, whilst a 5m resolution DEM, with a vertical error of 0.6m (Cripps, 2012), was used to quantify lake volume. Key uncertainties here relate to Holocene erosion and sedimentation, which potentially could lead to over or under estimation of the true volumes. Whilst the volume of Holocene alluvium within available accommodation space can be estimated from published data (e.g. Passmore et al., 2003) Holocene erosion is less well constrained. Therefore the contemporary topography was used to calculate material volumes and we handled the uncertainties by considering quantification at order of magnitude scales.

Field verification and sedimentology

As Roering et al. (2013) attest the availability of LiDAR data should not be a replacement for field work. Field verification of landforms is needed to inform geomorphologic interpretations and to avoid misinterpretation, with particular regards to equifinality. In this study multiple field trips were undertaken allowing an iterative approach to interpretative mapping, where field investigations appraised LiDAR data and vice versa. Both sides of the gorge, along the rim and in the valley bottom were extensively field walked. The number of sedimentary sections available in the study area was limited, but where possible the sedimentology associated with landform assemblages was described. In particular fluvial deposits within the gorge reach were targeted. Hand-augering surveys were also carried out to infer sub-surface topography beneath Holocene deposits, for example at Haydon Dean (Figure 1) and beneath Holocene alluvium within the Till gorge.

Study area description

The course of the Till valley from the Milfield Basin to its confluence with the River Tweed can be divided into two distinct reaches at Etal, where the Crookham-Etal kettle moraine complex, comprising eskers, kame and kettle topography, indicates a zone of stagnant ice during retreat of the Tweed Valley Ice Stream (Clapperton, 1971; Passmore and Waddington, 2009) (Figure 1). Downstream of Etal, the Till gorge cuts through the drumlised landscape of the Tweed valley. Upstream, the Milfied Plain basin contains extensive Holocene alluvium overlaying glacio-lacustrine deposits, at least two glacio-fluvial terrace levels (Passmore and Waddington, 2009) and deltaic sediments on the western side of the basin at the mouth of the Glen valley (Clapperton, 1971). The delta was deposited in Palaeolake Milfield, evidence for which includes over 22m of laminated clay and silt deposits interpreted as glacio-lacustrine sediments (Gunn, 1895). Quarry exposures revealed delta foresets (Payton, 1980) confirming a deltaic deposit dipping from an apex at 69m above sea level (asl) at the mouth of the Glen Valley to 40-42m asl at the terrace margins (Clapperton, 1971). These foresets are overlain (with an erosional contact) by approximately 2m of plane bedded sandy gravels interpreted as sub-aerial deposition by braided rivers (Payton, 1980). The delta surface is also characterised by palaeochannels eroded 1-3m into the terrace surface. A peat infill deposit within one such palaeochannel, the Galewood depression, was dated from 14,381-13,998 cal. BP to 13,415-13,255 cal. BP (Passmore and Waddington, 2009), the older, basal date providing a *post-quem* age of ca. 14 cal. BP for lake drainage. This is consistent with a radiocarbon date of 13,544-13,129 cal. BP from a palaeosol developed from glacio-lacustrine sediments located at 37m asl (Payton, 1980). This palaeosol was buried by approximately 2m of biogenic lacustrine sediments which led Payton to propose at least two phases of lake infilling, with a Younger Dryas rise in lake level invoked in addition to a Late-glacial lake. This contrasted with Clapperton's (1971) model of a gradual reduction in lake level controlled by Till gorge downcutting caused by outflow draining subglacially beneath stagnant ice in the Tweed Valley, with the incision of the rock-cut meanders reaching approximately modern channel elevations by the time of final ice retreat. Reviewing their more recent data alongside the previously published evidence, Passmore and Waddington (2009) concluded there is no basin-wide evidence for the Younger Dryas lake refilling model of Payton, and that the biogenic laminated sediments described must relate to ponding in a local depression. Passmore and Waddington (2009) suggest lake drainage and fluvial incision to 31.5m asl within a 2-3 ka period between disappearance of ice and the later part of the Windermere interstadial, and argue for episodic lowering due to the abandonment of the deltaic surface and the downvalley terrace levels. Missing from the models proposed to date is detailed consideration of the Till gorge geomorphology.

Results and geomorphological interpretation

Geomorphologic mapping of the Till gorge and surrounding landscape

The glacial lineations, predominantly drumlins (Clapperton, 1971; Everest et al., 2005; Clarke et al., 2004), are clearly identifiable on the LiDAR derived mapping (Figure 4) and trend along a main axis to 75°, reflecting the orientation of the Tweed Ice Stream as it deflected around the Cheviot Massif (Clapperton, 1971). The landscape of glacial lineations broadly slopes down to the River Tweed, the general decrease in elevation towards the

Tweed punctuated by drumlin summits. The Till gorge cuts through these glacial landforms along a main axis aligned to 310°, with an average slope of 0.002 (Passmore and Waddington, 2009). From Etal to the Tweed confluence the river length in the gorge is 10.53 km and is characterised by a meandering planform with a sinuosity index of 1.6. Meander bends at Mill Hill, Castle Heaton and Tindal have curvatures of radii of 50m, 75m and 85m respectively, whilst wider bends at Tiptoe and Heaton Mill have values of 175m and 245m. The mean meander wavelength along the gorge is 1070m, with average amplitude of 370m. Using a mean river channel width of 25m and a mean rim to rim gorge width of 280m the meander wavelength is 42.8 times the contemporary channel width and 3.8 times the gorge width, both values outside the usual reported range of 10-14 times channel width (Charlton, 2008).

The LiDAR data allowed terrace levels to be identified throughout the gorge. These include small features (< 10 m^2) and those obscured by vegetation or otherwise inaccessible for field investigation. Mapped terraces were assigned to three distinct levels on the basis of digitally extracted elevations from LiDAR. A lower terrace surface (T3) is located 3-5m above the contemporary River Till and is found on the inside of meanders and in zones of canyon expansion throughout the gorge. Coring reveals these to be benches of Holocene overbank slackwater flood deposits (cf. Benito et al., 2003) formed by Late Holocene alluviation rather than abandoned terrace surfaces caused by incision (Field, 2010). The highest terrace surface (T1) is primarily evident at three sites within the gorge - Tiptoe, Mill Hill and the Till-Tweed confluence (Figure 4), the Tiptoe and Mill Hill terraces in the widest sections of the gorge. These terrace surfaces occur approximately 15-20 m above the river level and individually are of greater areal extent, averaging 9.1×10^4 m^2 compared to the lower (T3) terrace mean of 1.6×10^3 m^2. A middle terrace (T2) can be identified at four reaches and is located 10-13 m above the contemporary river channel, with other possible surfaces between T2 and T1 on the right bank upstream of Mill Hill (Figure 4). At station 6.8 km a bedrock outcrop reveals the terrace here is cut into bedrock. At the Till-Tweed confluence the T1 and T2 terrace surfaces are inset within a fan-shaped deposit which is truncated by a 25m high scarp slope that runs parallel with the Tweed Valley (Figure 4). The scarp has been afforested and no sections were found to determine the thickness of sedimentary units sourced from the Till Valley.

The cross-sectional form and area of the eroded gorge varies spatially downstream (Figure 4). Its mean cross-sectional area is 4650 m^2, with a standard deviation of 2400 m^2. The greatest variability occurs between stations 4.46-8.40 km ranging from 3400 m^2 to over 10,000 m^2. Gorge area is generally lower than the mean within the upper and lower sections of the study reach, for example there is a general trend of decreasing cross-sectional area from station 5.73 km to the gorge entrance at Etal. Cross-sections extracted from the LiDAR DEM illustrate variations in form (Figure 5). Narrower, steep sided cross-sections (over 30m deep) occur mainly in the middle reach e.g. stations 8.40 km, 7.49 km and 4.46 km, although a narrow 30m canyon form is also evident at 2.15 km. In other zones the canyon widens, for example at stations 5.73 km and 3.77 km – these sites providing accommodation space for the T1 terrace surfaces. Lateral channels can be identified on the cross sections of the lower reach, for example stations 4.46 km, 3.77 km, 2.15 km, and 0.20 km, this latter palaeochannel located on the fan-shaped deposit at the mouth of the Till gorge.

In addition to the terrace surfaces, LiDAR reveals other previously unmapped geomorphic features. Fluvial bar features were identified at station 6.0 km at an elevation of 38-42 m asl inset within the gorge, and station 9.73 km at an elevation of 39-42m asl approximately 70m to the west of the gorge rim (Figure 5). A number of short and steep channels, interpreted as abandoned headcuts formed by knickpoint retreat (e.g. Baynes et al., 2015) and in places incising T1 terrace surfaces, can be identified on the LiDAR (Figure 4) despite often being subtle features or hidden by vegetation. At Tindal, between stations 8.5 and 9.5 km a series of abandoned headcuts are aligned in contrasting directions (to the NW and SE) split with a small stream entering the Till in a south-easterly direction at the apex of a gorge meander (Figure 4). Downstream two larger headcuts, aligned parallel to the gorge axis, can be seen at 7.0-7.5 km and 4.4-4.8 km) and a third probable headcut exists at Castle Heaton at 5.0-5.2 km (Figure 4).

One newly mapped glacial landform revealed through LiDAR is a meandering ridge extending northwards from the kettle moraine complex (Figures 3c, 3d and 4). The elevation of the ridge crest is from 64-74m. The relief of the feature has likely been subdued by ploughing and there are no exposures, however field walking indicates the presence of glacio-fluvial gravels. We interpret the ridge therefore to be an esker that would have connected to the kettle-kame-esker complex to the south-west prior to gorge formation. Finally, slumps and landslides, visible from the LiDAR data, were identified along the gorge, for example at 6.4-6.6 km, 5.1-5.3 km and possibly at 4.1-4.3 km. The presence of an abandoned quarry and associated spoil makes interpretation of this latter site speculative.

Sedimentary evidence

Available exposures are limited in the gorge reach, however a section (Figure 6) excavated next to the dyke on the north bank of the river (station 5.0-5.1 km) revealed imbricated boulders of local sandstone and dyke bedrock deposited in beds of rounded gravels, within a matrix of coarse sand to granules matrix, and units of well sorted pea-size gravels, and fine sands. The sorted gravels and sands indicate water lain deposition, whilst high energy processes are required to erode and imbricate the local bedrock clasts. The deposit is located at 21-23m asl which places it inset below the T1 terrace surface (30-32m asl) and above the T3 fine grained Holocene alluvium (18-19m asl). The bar feature at Tiptoe (6.0 km station) is located topographically higher than the T1 terrace level (30-32m) and its planform can be linked to the elliptical shape of the T1 surface at this reach. No sections exist but soil augering revealed the presence of gravels beneath the topsoil (Cripps, 2012). The bar at 9.73 km is located at the elevation of the gorge rim, but 70m to the east (see Figure 5i). Small sections in the bar surface reveal sorted pebbles, that combined with its planform morphology and spatial relationship to the gorge suggests the deposit is a small scale run-up bar feature as described at the mega-flood scale by Herget (2005).

Coring of Holocene alluvium within the gorge revealed an undulating gravel, boulder (and/or bedrock) sub-surface topography. Excavation of a pit into the uppermost gravels at station 7.7 km revealed the surface of these coarse deposits to be at approximately 24 m asl. The deposit comprised angular cobbles with imbrication indicating northerly flow, within a granular matrix exhibiting dune cross bedding, interpreted as overbank deposition of high energy gravels on the inside of the meander bend. At 6.5-6.8 km a bar and buried channel were revealed beneath the Holocene alluvium (Field, 2010). Finally, the gorge is littered with large, sub-rounded boulders of local sandstone, on T1 and T2, as well as within the contemporary channel and sometimes revealed at the base of Holocene alluvium (T3) by scouring during recent floods. Whilst some boulders are clearly the result of rock falls, in places, for example the inside of the Tindal meander bend between stations 8.7-8.8 km, isolated boulders appear to have been fluvially transported with imbrication demonstrating down valley flow.

Assessing a sub-glacial model of gorge formation

Clapperton (1971) noted the lack of glacio-lacustrine sediments in kettle holes of the Crookham-Etal moraine complex and surmised the contemporaneous presence of stagnant ice and Palaeolake Milfield. This observation was used to infer gorge formation through sub-glacial drainage from the lake, however there is no evidence for stagnant ice in the zone between Etal and the River Tweed or glacial deposits within the gorge – truncated tills are exposed at some locations along the gorge rim. The LiDAR mapping does extend the area of the kettle-kame-esker complex northwards (Figure 4) but not sufficiently far to suggest ice over the drumlinised area contemporaneously with the stagnant ice associated with the kettle moraine. Assuming a continuous sedimentary deposit from the newly mapped esker ridge to the kettle moraine complex, and/or the presence of stagnant ice in the immediate vicinity, we can hypothesize the lake would have been dammed here between 60 and 70m, which correlates with the sediment-landform evidence for the lake stand reviewed by Clapperton (1971). However, subglacial drainage of the lake need not be inferred as sub-aerial outflow at Haydon Dean to the north east of Etal (Figure 1) would have been possible once ice decoupled from the escarpment to the east of the Milfield basin. Coring at the entrance to Haydon Dean (Figure 1) revealed over 4m of Holocene peat and silts infilling the channel with a bedrock lip (a continuation of the dyke exposed in the gorge) identified at 62m asl which would indicate a minimum lake level, the actual lake level dependent on the unknown, and likely seasonally variable, water depth at this outflow (Cripps, 2012). Thus we propose there was no Tweed Valley drainage route from Palaeolake Milfield, the combination of stagnant ice and the esker-kettle moraine complex dammed the lake to the SE of the drumlinised landscape, with outflow drainage through Haydon Dean.

Further geomorphic evidence leading Clapperton (1971) to argue for sub-glacial drainage was the gorge entrance at Etal, with a bedrock lip at an elevation of 42m, within the kettle moraine zone (station 10.2-10.6 km). Our analysis of gorge morphology (Figure 5) shows a cross-sectional area of 2120 m^2 at Etal compared to a mean area of 4560 m^2 for the whole gorge, and along the majority of the reach the gorge rim elevation is above 42m. For example between stations 9.2-4.3 km the rim is consistently above 50m with the maximum elevations between stations 8.6-7.0 km (where mean elevation is 53.6m asl), the section adjacent to the newly mapped esker ridge (7.6-7.9 km). We argue therefore that gorge morphology, in combination with the landforms and sedimentary evidence described above, can be better explained by a GLOF with the breach located in the zone 7.6-7.9 km. Under this hypothesis gorge erosion from the breach site to Etal occurred by knick-point retreat (Baynes et al., 2015), this explaining the upstream reduction in cross-sectional area to ca. 2000 m^2 at the Etal reach as discharge waned as the event proceeded. A modern analogue flood from Canyon Lake Reservoir (USA) provides evidence for rapid bedrock incision. Lamb and Fonstad (2010) report average vertical incision of 7m in three days due to bedrock plucking during a flood of <1500 m^3s^{-1}.

Event synthesis and palaeohydraulic reconstruction

Synthesising the geomorphic evidence (Figure 7 and Table 1) we identify a two phase outburst event (Figure 8) triggered when Palaeolake Milfield (Figure 11a), at a minimum elevation of 63 m asl (assuming a 1m flow depth at the Haydon Dean lake outflow), breached an esker dam between stations 7.6-7.9 km (Figure 7). Using Costa and Schuster's (1988) empirical equation for dam break floods (see Table 1) based on dam height and lake volume we estimate a peak flow of 1065-3140 m^3/s for a lake volume of 1.7 x 10^9 m^3 and assuming minimum and maximum dam heights of 12-22m constrained by the LiDAR DEM (the actual height is unknown due to erosion at the breach site). The water flowed across the drumlinised landscape towards the River Tweed, encountering landform obstacles *en route* causing local variations in flow pathway, such as at Castle Heaton (ca. 50m asl) where the intake for one of the downstream abandoned headcuts and a lateral channel are located, the latter passing between drumlins to the NE of the gorge (Figure 8b). At Mill Hill flow was impeded by the higher relief (Figure 7) with the floodwater bypassing the drumlin over a spillway at ca. 40-42 m asl to the NE, before taking a sharp turn to the SW, to flow north of Mill Hill (Figure 8b). At the calculated peak discharges, the accommodation space for the water above the subsequently eroded gorge would take 2.2-6.5 hours to fill prior to bypassing Mill Hill via the spillway to the NE. Making the assumption that the Mill Hill spillway controlled the flow rate of the event we estimated flow discharge over the spillway, using flow hydraulics, specifically the general form of equation for flow over a weir (Chow, 1958: Equation 14-9, p362 – see Table 1 caption for a fuller explanation). The results from modelling a range of water depths up to 3m, the depth at which other cols may have been overtopped according to the modern DEM, and H/h constants <10 (the usual reported range according to Chow, 1958) were discharges of 133-1512 m^3/s. Due to the flow attenuation evidence by the flow blockage and eddying we therefore applied lower and upper order of magnitude estimates of 100-1000 m^3/s (Table 1), the former considered conservative. These flow estimates provide a range of 14-126 days for lake level to fall from 60 to 45 m asl. During this period 2.3-4.7 x 10^7 m^3 of glacial till and bedrock material was eroded down to the T1 terrace level at a mean rate of incision of 0.04-0.37 m/day, with a sediment yield of 4-80 x10^7 $t/km^2/yr$ (Table 2).

The temporary flow blockage at Mill Hill accounts for the large T1 terrace surfaces located upstream of this point as evidenced by the low T1 gradient (Figure 7). This back-flooding, probably coupled with a higher rock lip created by the resistant dyke at 5.0 km, is particularly evident at Tiptoe (5.4-6.0 km) where the gorge planform is elliptical in shape reflecting eddying, the shape and orientation of the bar at 6.0 km (Figure 4) interpreted as flow separation at the boundary of the eddy and incoming floodwater. Whilst the geomorphological setting is not directly analogous, Carrivick et al. (2013) noted flow recirculation and flood attenuation associated with a 2008 GLOF in western Greenland - the flow pathway of that event characterised by a bedrock cascade with intermediary lakes.

The Mill Hill spillway flow route functioned until Phase 2, when Mill Hill was breached at stations 2.1-2.3 km (Fig 7b). Estimating a likely dam height of 8m from the LiDAR DEM and elevation of the upstream T1 terrace level, and assuming a lake volume of 2.8 x 10^8 m^3 based on the volume at the 45m lake level plus the volume of water estimated in the gorge (the accommodation space between the Phase 1 erosion and the 42 m water level controlled by the spillway), produces a discharge estimate of 421 m^3/s. In Table 1 we therefore use an order of magnitude constraint of 10^2-10^3 m^3/s to constrain Phase 2 event duration. The Phase 2 event therefore would take 3-22 days until complete lake drainage. During this phase, 8.2-17 x 10^6 m^3 of material was eroded, with a mean incision rate of 0.29-2.87m and sediment yield of 2-33 x10^8 t/km^2/day. This suggests a greater rate of vertical incision than during Phase 1, a finding consistent with the geomorphic evidence – note the gorge depth data presented in Figure 9a and the greater evidence of lateral erosion during Phase 1 (e.g. the Tiptoe eddy).

Phase 2 explains the presence of multiple terrace levels, with the T1 surfaces preserved following the second phase of incision triggered at stations 2.1-2.3 km (Figure 2). The occurrence of abandonded headcuts incised into the gorge rim (Figures 4 and 7) and T1 terrace (Figure 4) can also be explained by the flood incising multiple routes into each of these surfaces during a two stage event. Phase 2 included another breach point at the apex of the Mill Hill meander (3.0-3.2 km) accounting for its low radius of curvature. Note the headcut channels, scarp slopes and T2 terrace levels all dipping towards the bend apex

(Fig 7b). Rapid and catastrophic incision at the dyke reach is also suggested by the sedimentary section at station 5.0 km (Figure 6), which is inset between the T1 and T3 terraces, implying association with the abandonment of the T1 surface.

This double breach event is evident in the contemporary gorge topography by the mean gorge depth data presented in Figure 9a, which highlights greatest gorge depth at the breach sites. Whilst the timing of the Phase 2 breach relative to the initial breach is uncertain, the balance of evidence from the elevation and location of headcut channels (Figures 4, 7 and 8) and T1 terrace levels suggests lake level could have dropped to around 45m before the Phase 2 breach. Furthermore no geomorphic or sedimentary evidence to suggest a lake still stand of any significant duration controlled by a 40-42m spillway was found.

To summarise our event synthesis, given the LiDAR mapping supports a GLOF interpretation, we were able to constrain an order of magnitude estimate of flood duration based on an iterative process informed by simple flow calculations, spatial volume data and the geomorphic evidence. This analysis provides an event duration of 16.5-155 days (the latter considered conservative), during which 3.1-6.4 x 10^7 m^3 of material was eroded (Fig. 8b) to form the gorge (1.9-3.8% of the original lake volume) with a sediment yield of 42-798 x 10^6 $t/km^2/yr$ (Table 2). This relatively long duration compared with many observed GLOFs is likely the result of the low relief setting of the Till Gorge, and relatively shallow Palaeolake Milfield,compared to contemporary GLOFs in steeper mountain regions.

Discussion

The geomorphological mapping presented herein demonstrates that analysis of high resolution LiDAR has the potential to reveal the occurrence of past low magnitude (<10^5 m^3s^{-1}) Late Quaternary GLOFs in the landscape, by identifying small or obscured landforms that aid interpretation and allow hypothesis testing. This suggests such events could be under-represented in Quaternary mapping, and further GLOF sites may be identified by reinvestigating palaeolake sites, such as Murton and Murton's (2012) overview of lowland Quaternary palaeolakes in the UK. LiDAR-based mapping therefore has the potential to increase Quaternary GLOF inventories, which has relevance for their spatial distribution and their frequency of occurrence in deglacial landscapes. Enhanced knowledge of meltwater processes during the decay of palaeo-ice sheets can help improve understanding of contemporary ice sheet dynamics. The storage and catastrophic release of meltwater from ice- and moraine-dammed lakes is increasingly shown to be a crucial component of ice-to-ocean water and sediment flux (Carrivick and Tweed, 2013) and whilst the role of megafloods on climate, through their impact on ocean circulation, has been discussed (e.g. Broecker, 2006; Teller et al., 2002) regional palaeohydrological balances between meltwater storage in proglacial lakes (Carrivick and Tweed, 2013), pro-glacial riverine discharge and outburst events are poorly constrained. There is therefore the need for regional high resolution mapping to better constrain types of, and processes associated with, meltwater drainage pathways.

In this paper, the application of LiDAR mapping has revealed a suite of small scale landforms indicative of a relatively low magnitude outburst event, including abandoned head-cuts, run-up bars, eddy circulation features and terrace surfaces. Whilst it is the suite of landforms that has helped infer a GLOF, the identification of small-scale features such as the run-up bars and eddy-related landforms (Figures 3e, 3f and 10), show the value of LiDAR for identifying unanticipated landforms (Roering et al., 2013) that can lead to reinterpretations of formative processes. Indeed the geomorphic evidence of contemporary (e.g. Anacona et al., 2015) and Quaternary GLOFs indicates uniqueness in the landscape signatures of individual outburst events. This reflects variability in geology (resistance to erosion), topographic and geomorphological settings, including dam type and size; glacier dynamics; lake size and morphology; and meltwater pathways (e.g. Carling et al., 2009a, 2009b). This landform variability further highlights the requirement for high resolution digital mapping to decipher meltwater processes from geomorphic evidence in previously glaciated landscapes, though ground-truthing is essential in this process to confirm complex landform interpretations (Roering et al, 2013).

The spatial scale issues of identifying relatively small magnitude GLOFs are highlighted in Figure 10, which shows part of the upper reach of the Till gorge at four different resolutions: the 1m and 2m LiDAR and 5m and 10m resolutions resampled from the 1m LiDAR. Some of the diagnostic landform evidence used to infer an instantaneous outburst event disappears at the lower resolutions, notably the run-up bar, the eddy terrace, other small terraces and the flow pathways dipping into the gorge. Whilst the 5-10m DEMs can be used to locate potential moraine- or ice-dammed lakes and outburst pathways, the results presented herein suggest higher resolution LiDAR is needed to identify the potential complexities in the history of these drainage pathways, necessary for elucidating landscape-scale genetic processes using process-form relationships inferred from small scale landforms. For example, the 10m DEM is of sufficient resolution to identify the major headcuts along the Till flood pathway, suggesting outburst flow across the drumlin field, but the detail of the two phase outburst event, evident in complex terrace levels and the run-up bar features, requires LiDAR data. This is especially so where forest obscures the geomorphology (e.g. Lin et al., 2013) as is the case for significant areas of the Till gorge. Our recommendation therefore is that lower resolution DEMs are used to scope locations of potential ice marginal lake basins and drainage pathways, followed by mapping of potential outburst flood sites with high resolution LiDAR data. As noted by Roering et al. (2013) whilst desktop mapping may be viewed as desirable from a time-cost perspective, fieldwork is required to confirm landform interpretation. For example, in this study, fieldwork confirmed diagnostic evidence of catastrophic flow both within the gorge (Figure 6), and at the gorge rim (the run-up bar in Figures 4, 5 and 10). We also found that an iterative approach where multiple field trips and subsequent re-mapping using desktop LiDAR helped refine the inferred event sequence.

Palaeohydrological evidence can be used to delineate ice margins, as lake basins and their outflows are necessarily ice free, and the change in outflows can reveal retreat patterns. This approach has been applied to ice-dammed lakes in other low relief landscapes, particularly in the former Laurentide Ice Sheet region (e.g. LaRocque et al, 2003a; 2003b; Jansson, 2003). Figure 12a shows hypothesised ice margins of the Tweed Valley ice stream as identified through this combination of palaeohydrological and glacial geomorphological evidence. Palaeolake Milfield is shown alongside other palaeolakes identified through the regional DEM and LiDAR, on the basis of evidence outlined below. Of relevance to geomorphic response in the Till Valley is Palaeolake Bowmont, which has been identified on the basis of LiDAR derived palaeo-shorelines and delta surfaces, with an abandoned quarry revealing delta foresets in section (Figure 12c). Figure 12c shows this lake was dammed by a moraine, as mapped by BRITICE (Clark et al., 2004). The shoreline evidence and spillway, subsequently used for an incline on the now disused Cornhill-Alnwick railway, provide evidence for a lake level at ca. 85m asl, which according to contemporary topography would suggest an ice margin across the Bowmont-Tweed watershed (ca. 70m asl). On the north side of the Tweed Valley (Figure 12a), the lowland tributary River Leet (113 km^2) flows in a contrary direction to the Tweed Valley through an incised gorge ca. 15m deep and ca. 100m wide, which becomes asymmetrical in its lower reach. Our palaeohydrological interpretation is that there was an ice margin here which resulted in an ice dammed lake within the drumlin field, with drainage causing incision of the gorge and subsequent ice marginal flow resulting in the asymmetrical cross sections. Analysis of LiDAR mapping reveals a small depression (0.06 km^2) with a short incised drainage pathway aligned up-valley and at right angles to the proposed ice margin (Figure 12a). We suggest this is the topographic signature of GLOF drainage of a small lake dammed at the ice margin.

The identification of GLOFs has implications for regional landscape development and fluvial system response to post-glacial environmental change. For example, the incision phase of regional paraglacial response, previously considered to have occurred over *ca.*3000 years (Passmore and Waddington, 2009) prior to ca. 14,000 cal. BP, has to be reassessed assuming a new interpretation that incision was achieved by lake drainage during the Till GLOF. The mechanisms of erosion within the lake basin during the GLOF can be hypothesised to be the result of knick-point retreat by lake bottom waters and eddying (see the National Geographic’s (2011) video of Condit dam removal on the White Salmon River, Washington State, USA for a modern analogue), combined with inflow drainage experiencing a rapid fall in base level. Projecting falling lake levels onto modern topography reveals exposed land surfaces starting to appear sub-aerially (Figure 11a). The morphology of this subsurface topography explains features such as the large Crookham meander, as well as the two palaeochannels indicated in Figure 11b that we interpret as abandoned headcut channels progressing by knick point retreat into the lake basin until the channel occupying the eventual Holocene meander belt of the River Till captures the flow. The terrace surfaces interpreted by Clapperton (1971) and Passmore and Waddington (2009) as re-worked sands and gravels of the Glen delta, linked to the erosive braid channels identified by Payton (1980), are likely to be so but it was the flow circulation during lake fall that carried out this geomorphic work. Figure 13 shows how abandoned palaeochannels on the Glen delta can be explained under a flood hypothesis, with rapid channel incision by the proto-Glen grading the channels to progressively lower lake levels as flow was diverted around emerging topography. The NE aligned Lanton palaeochannel graded to 55 m asl, and the Galewood palaeochannel to 52 m asl. The emerging topography of the delta coupled with the Glen Valley inflow discharge orientated the Galewood and proto-Glen channels further to the east than the Lanton palaeochannel. We argue that in addition to the orientation of the palaeochannels, the morphology of scarp slopes and slumped material (Figure 13) can be explained more coherently by a rapid lake level drop rather than longer term meltwater processes, although slumping could also be affected by periglacial activity. We concur with Passmore and Waddington (2009) regarding a paraglacial response with the river adjusting to changes in sediment load and discharge regime, however in line with the GLOF hypothesis the reworking of coarse sediment in the Till basin would have dominated rather than net incision.

One added complication to the history of landscape development in the Milfield basin is the occurrence of an upstream GLOF from Palaeolake Bowmont (Figure 12c). The timing of the Bowmont GLOF is unknown but given the shoreline and delta evidence for an 85 m lake elevation and the lack of evidence for a lower stand it is likely the event occurred when ice was still present at the Bowmont-Tweed watershed at 70m (see Figure 12a). However, we have been unable to map unequivocal geomorphic or sedimentary evidence that enables the relative chronology of the Till and Bowmont GLOFs to be established. One speculative hypothesis is that the Bowmont breach and flood may have triggered the Till outburst if the flood wave reached the northern end of palaeolake Milfield with sufficient energy to overtop and breach the esker dam at Tindal. Irrespective of the relative timing, the breach of this moraine would have opened up meltwater pathways and sediment delivery from the Bowmont catchment, thus altering discharge and sediment regimes into the Milfield Plain.

Another consequence of the Till GLOF is that the event is likely to have also had an impact downstream, in particular through a high sediment flux. Indeed, despite the relatively low magnitude discharge reconstructed for the event in comparison to Quaternary megafloods, in terms of its specific yield, which we quantify to be in the order of $x10^7$-$10^9 m^3/km^2/yr$, the Till GLOF can be classed as an extreme sediment delivery event – defined as greater than x 10^4 $m^3/km^2/yr$ by Korup (2012). One impact of this sediment delivery event is likely to have been the temporary blockage of the Tweed Valley by the fan deposit (Figure 4), damming drainage upstream towards the ice margin. The Tweed Valley is a focus of ongoing research to establish whether the morphology of the lower gorge reach of the river was formed either as a sub-glacial tunnel valley (Kehew et al., 2012) by multiple outburst floods or by a combination of both sub-glacial meltwater and subsequent sub-aerial pathways, including GLOFs.

Considering LiDAR research more broadly, this study provides an example of the value of LiDAR mapping for improving our understanding of timescales and event frequency in geomorphology. Whilst progress in Quaternary geochronology improves constraints on the absolute chronology of landscape development, for elucidating the rate and timing of geomorphic processes, in the case of geologically near-instantaneous GLOFs it is the geomorphological mapping that provides the critical evidence for deciphering a single geomorphic event. Our study, through increasing the GLOF inventory for one particular area of the palaeo-Tweed Valley ce stream, demonstrates an increased frequency of GLOFs in the lower Tweed basin, and in the case of the Till flood an extreme sediment delivery event. This work therefore adds to the growing literature (e.g. Begg and

Mouslopoulou, 2010; Van Den Eeckhaut et al., 2010; Lin et al., 2013) where improved spatial mapping from higher resolution LiDAR derived DEMs leads to improved geomorphological understanding of the frequency of occurrence of geomorphological events in the landscape.

Conclusion

In this paper we have presented LiDAR based geomorphological mapping that reveals evidence for low magnitude (ca. 10^2-10^4 m^3/s) GLOFs associated with the retreating Tweed Valley ice stream during the deglaciation of the British-Irish Ice Sheet. In particular we focused on the Till gorge (NE England) formed when a proposed esker dam was breached releasing floodwaters from Palaeolake Milfield. Using discharge estimates and spatial lake volume data the GLOF and gorge formation was constrained to between 16.5-155 days' duration, the latter figure considered a conservative estimate based on the lowermost order of magnitude flow estimates. The Till GLOF can be classified as an extreme sediment yield event (cf. Korup, 2012), with estimated rates constrained to the order of 10^7-10^9 $m^3/km^2/yr$. The event was important for regional palaeography in creating a new tributary pathway to the lower River Tweed. The route of the proto-Till has yet to be investigated but one possibility, according to the regional DEM and geomorphic mapping, is that stagnant ice and the unconsolidated sediments of the kettle moraine complex to the west of Crookham (Figure. 1) blocked a previous connection between the Milfield Basin and River Tweed. Mapping of incised meltwater pathways and proglacial lakes has been used to define the likely position of the Tweed ice stream margin at the time of deposition of the Crookham kettle moraine complex.

The paper demonstrates that high resolution LiDAR mapping is an important tool for determining specific meltwater processes, for example deciphering between sub-glacial versus sub-aerial meltwater flow and elucidating geologically instantaneous events. Meltwater pathways can be mapped using 5-10m resolution DEMs (e.g. Britice GIS, Clarke et al., 2006), however we recommend the use of LiDAR data to decipher their specific processes of formation. Carrying out regional mapping of meltwater pathways and palaeolake storage at high resolutions will help constrain regional palaeohydrological balances between meltwater storage versus contribution to oceans (Carrivick and Tweed, 2013). The mapping hererin presents evidence of a greater frequency of regional GLOFs in the landscape than hitherto identified and therefore helps build a more complete picture of landscape dynamics at ice margins, with particular regards to the initiation and cessation of water and sediment pathways associated with valley damming and dam breach events (Carrivick and Tweed, 2013). The recognition of outburst events and the geomorphic work carried out has implications for post-glacial landscape development and fluvial system response. We propose the Till GLOF promoted rapid knick-point retreat into the Milfield Plain basin creating abandoned palaeochannels and terraces, whilst the Bowmont breach opened up a new meltwater and sediment pathway into the basin thus influencing paraglacial response (Passmore and Waddington, 2009). Finally, we hypothesise that the Till outburst flood caused damming of the lower Tweed through the creation of a fan deposit blocking the Tweed a few kilometres downstream of our reconstructed ice margin.

Acknowledgements

VT is especially grateful to Dave Passmore (University of Toronto) for supplying 2m LiDAR data from his Milfield Basin research which led to initial research in the Till gorge. The 1m and 2m LiDAR data sets used for this research were provided by Geomatics Ltd. Figures 1, 11a and 12a contain Ordnance Survey data © Crown copyright OS Terrain 50 (2013).. The authors would like to thank MSc students Alex Field and Chris Oldknow for fieldwork in the Till gorge. Jenny Kynaston of the Department of Geography (Royal Holloway University of

London) designed the layout of the figures. We thank Ron and Sonia Thorndycraft for their logistical support of this unfunded research. Finally, we wish to thank two anonymous reviewers for their thoughtful comments that have helped improve the clarity of the manuscript.

References

Alho P, Baker VR, Smith LN. 2010. Paleohydraulic reconstruction of the largest Glacial Lake Missoula draining(s). *Quaternary Science Reviews* **29**: 3067-3078.

Anacona PI, Mackintosh A, Norton KP. 2015. Hazardous processes and events from glacier and permafrost areas: lessons from the Chilean and Argentinean Andes. Earth Surface Processes and Landforms **40**: 2-21.

Baker VR. 2009. The Channeled Scabland: a retrospective. *Annual Review of Earth and Planetary Science* **37**: 393-411

Baker VR, Benito G, Rudoy AN. 1993. Palaeohydrology of late Pleistocene superflooding, Altai mountains, Siberia. *Science* **259**: 348-350.

Baynes ERC, Attal M, Niedarmann S, Kirstein LA, Dugmore AJ, Naylor M. 2015. Erosion during extreme flood events dominates Holocene canyon evolution in northeast Iceland. *Proceedings of the National Academy of Science*. DOI: 10.1073/pnas.1415443112

Begg JG, Mouslopoulou V. 2010. Analysis of late Holocene faulting within an active rift using lidar, Taupo Rift, New Zealand. *Journal of Volcanology and Geothermal Research* 190: 152-167.

Benito G, O'Connor JE. 2003. Number and size of last-glacial Missoula floods in the Columbia River valley between the Paco Basin, Washington and Portland, Oregon. *Geological Society of America Bulletin* **115**: 624-638.

Benito G, Sánchez-Moya Y, Sopeňa A. 2003. Sedimentology of high-stage flood deposits of the Tagus River, Central Spain. *Sedimentary Geology* **157**: 107-132.

Broecker WS. 2006. Abrupt climate change revisited. *Global and Planetary Change* **54**: 211-215.

Brown AG. 2008. Geoarchaeology, the four dimensional (4D) fluvial matrix and climatic causality. *Geomorphology* **101**: 278-297.

Carling PA, Herget J, Lanz JK, Richardson K, Pacfici A. 2009a. Channel-scale erosional bedforms in bedrock and in loose granular material: character, processes and implications. In *Megaflooding of Earth and Mars,* Burr DM, Carling PA, Baker VR (eds) Cambridge University Press: Cambridge; 13-32

Carling PA, Burr DM, Johnsen TF, Brennand TA. 2009b. A review of open-channel megaflood landforms on Earth and Mars. In *Megaflooding of Earth and Mars*, Burr DM, Carling PA, Baker VR (eds) Cambridge University Press: Cambridge; 33-49 [

Carling PA, Villanueva I, Herget J, Wright N, Borodavko P, Morvan H. 2010. Unsteady 1D and 2D hydraulic models with ice dam break for Quaternary megaflood, Altai Mountains, southern Siberia. *Global and Planetary Change* **70**: 24-34.

Carrivick JL, Quincey DJ. 2014. Progressive increase in number and volume of ice-marginal lakes on the western margin of the Greenland Ice Sheet. *Global and Planetary Change* **116**: 156-163.

Carrivick JL, Turner AGD, Russell AJ, Ingeman-Nielsen T. Yde, JC. 2013. Outburst flood evolution at Russell Glacier, western Greenland: effects of a bedrock channel cascade with intermediary lakes. *Quaternary Science Reviews* **67**: 39-58.

Carrivick JL, Tweed FS. 2013. Proglacial lakes: character, behaviour and geological importance. *Quaternary Science Reviews* **78**: 34-52.

Charlton R. 2008. *Fundamentals of Fluvial Geomorphology*. Routledge. 234pp.

Chow VT. 1959. *Open-channel Hydraulics*. Mcgraw-Hill Kogakusha Ltd. 680pp.

Clapperton CM. 1971. The pattern of deglaciation in north Northumberland. *Transactions of the Institute of British Geographers* **53**: 67-78.

Clarke G, Leverington D, Teller JT, Dyke AS. 2003. Superlakes, megafloods and abrupt climate change. *Science* **293**: 283-287.

Clarke G, Leverington D, Teller JT, Dyke AS 2004. Paleohydraulics of the last outburst flood from glacial Lake Agassiz and the 8200 BP cold event. *Quaternary Science Reviews* **23**: 389-407.

Clarke CD, Evans DJA, Khatwa A, Bradwell T, Jordan CJ, Marsh SH, Mitchell WA, Bateman MD. 2004. Map and GIS database of glacial landforms and features related to the last British Ice Sheet. *Boreas* **33**: 359-375.

Clayton JA, Knox JC. 2008. Catastrophic flooding from Glacial Lake Wisconsin. *Geomorphology* **93**: 384-397.

Cloke J, Todd P, Thompson C, Watson F, Denham R., Khanal G. 2013. The use of multi temporal LiDAR to assess basin-scale erosion and deposition following the catastrophic January 2011 Lockyer flood, SE Queensland, Australia. *Geomorphology* **184**: 111-126.

Costa JE, Schuster RL. 1988. The formation and failure of natural dams. *Geological Society of America Bulletin* **100**: 1054-1068.

Cripps JE. 2012. *Quantifying the palaeohydrology of Glacial Lake Milfield and its outburst flood drainage: Implications for landscape evolution of the Till Valley (NE England)*. Unpublished MSc dissertation, University of London. 71pp.

Denlinger RP, O'Connell DRH. 2010. Simulations of cataclysmic outburst floods from Pleistocene Glacial Lake Missoula. *Geological Society of America Bulletin* **122**: 678-689

Dussaillant A, Benito G, Buytaert W, Carling P, Meier C, Espinoza F. 2010. Repeated glacial-lake outburst floods in Patagonia: an increasing hazard? *Natural Hazards* **54**: 469-481.

Everest J, Bradwell T, Golledge N. 2005. Subglacial landforms of the Tweed Palaeo-ice-stream. Scottish Landform Example 35. *Scottish Geographical Journal* **121**: 163-173

Field A. 2010. Investigating the application of palaeoflood hydrology in a UK context: the River Till (NE England). Unpublished MSc thesis, University of London.

Glenn NF, Streutker DR, Chadwick DJ, Thackray GD, Dorsch J. 2006. Analysis of LiDAR-derived topographic information of characterizing and differentiating landslide morphology and activity. *Geomorphology* **73**: 131-148.

Gunn W. 1895. *The geology of part of Northumberland, including the country between Wooler and Coldstream*. Memoirs of the Geological Society of Great Britian. HMSO, London.

Helm V, Humbert A, Miller H. 2014. Elevation and elevation change of Greenland and Antarctica derived from CryoSat-2. *The Cryosphere* **8**: 1539–1559.

Herget, J. 2005. Reconstruction of Pleistocene ice-dammed lake outburst floods in the Altai Mountains, Siberia. *Geological Society of America Special Paper* **386**: 118pp.

Hurst, MD, Mudd, SM, Walcott R, Attal M, Yoo K. 2012. Using hilltop curvature to derive the spatial distribution of erosion rates. *Journal of Geophysical Research* **117**: FO2017.

Hydrologic Engineering Center 2011. *HEC-GeoRAS – GIS tools for support of HEC-RAS using ARCGIS. User's Manual*. Version 4.3.93. US Army Corps of Engineers. 244pp.

IPCC. 2013. Summary for Policymakers. In: *Climate Change 2013: The Physical Science Basis. Contribution of Working Group I to the Fifth Assessment Report of the Intergovernmental Panel on Climate Change,* Stocker TF, Qin D, Plattner G-K, Tignor M, Allen SK, Boschung J, Nauels A, Xia Y, Bex V, Midgley PM (eds.). Cambridge University Press, Cambridge, United Kingdom and New York, NY, USA.

Jansson KN. 2003. Early Holocene glacial lakes and ice marginal retreat pattern in Labrador/Ungava, Canada. *Palaeogeography, Palaeoclimatology, Palaeoecology* **193**: 473-501.

Kattelmann R. 2003. Glacial lake outburst floods in the Nepal Himalaya: a manageable hazard. *Natural Hazards* **28**: 145-154.

Kehew AE, Piotrowski JA, JØrgensen F. 2012. Tunnel valleys: Concepts and controversies – A review. *Earth-Science Reviews* **113**: 33-68.

Kershaw JA, Clague JJ, Evans SG.. 2005. Geomorphic and sedimentological signature of a two-phase outburst flood from moraine-dammed Queen Bess Lake, British Columbia, Canada. *Earth Surface Processes and Landforms* **30**: 1-25.

Korup O. 2012. Earth's portfolio of extreme sediment transport events. *Earth-Science Reviews* **112**: 115-125.

Korup O, Tweed F. 2007. Ice, moraine, and landslide dams in mountainous terrain. *Quaternary Science Reviews* **26**: 3406-3422.

LaRocque A, Dubois J-MM, Leblon B. 2003a. A methodology to reconstruct small and short-lived ice-dammed lakes in the Appalachians of Southern Québec. *Quaternary International* **99-100**: 59-71.

LaRocque A, Dubois J-MM, Leblon B. 2003b. Characteristics of late-glacial ice-dammed lakes reconstructed in the Appalachians of Southern Québec. *Quaternary International* **99-100**: 73-88.

Lamb MP, Fonstad MA. 2010. Rapid formation of a modern bedrock canyon by a single flood event. *Nature Geoscience* **3**: 477-481.

Lin Z, Kaneda H, Mukoyama S, Asada N, Chiba T. 2013. Detection of subtle tectonic-geomorphic features in densely forested mountains by very high-resolution airborne LiDAR survey. *Geomorphology* **182**: 104-115.

Mackey BH, Roering JJ, Lamb MP, 2011. Landslide-dammed paleolake perturbs marine sedimentation and drives genetic change in anadromous fish. *Proceedings of the National Academy of Sciences* **108**: 18905-18909.

Margold M, Jansson KN, Stoeven AP, Jansen JD. 2011. Glacial Lake Vitim, 3000 km3 outburst flood from Siberia to the Arctic Ocean. *Quaternary Research* **76**: 393-396.

Marren PM. 2005. Magnitude and frequency in proglacial rivers: a geomorphological and sedimentological perspective. *Earth-Science Reviews* **70**: 203-251.

McKillop RJ, Clague JJ. 2007a. Statistical, remote sensing based approach for estimating the probability of catastrophic drainage from moraine-dammed lakes in southwestern British Columbia. *Global and Planetary Change* **56**: 153-171

McKillop RJ, Clague JJ., 2007b. A procedure for making objective preliminary assessments of outburst flood hazard from moraine-dammed lakes in southwestern British Columbia. *Natural Hazards* **41**: 131-157.

Murton DK, Murton JB. 2012. Middle and Late Pleistocene glacial lakes of lowland Britain and the southern North Sea Basin. *Quaternary International* **260**: 115-142.

Murton J, Bateman M, Dallimore S, Teller J, Yang Z. 2010. Identification of Younger Dryas outburst flood path from Lake Agassiz to the Arctic Ocean. *Nature* **46**: 4740-743.

National Geographic (2011). http://video.nationalgeographic.com/video/news/us-condit-dam-breach-vin. Last accessed: September 24th 2014.

Notebaert B, Verstraeten G, Govers G, Poesen J. 2009. Qualitative and quantitative applications of LiDAR imagery in fluvial geomorphology. *Earth Surface Processes and Landforms* **34**: 217-231.

Oguchi T, Hayakawa YS, Wasklewicz T. 2011. Data Sources. *Development in Earth Surface Processes* **15**: 189-224.

Passmore DG, Waddington C. 2009. Paraglacial adjustment of the fluvial system to Late Pleistocene deglaciation: the Milfield Basin, northern England. Geological Society, London, Special Publications **320**: 145-164.

Passmore DG, Waddington C., Houghton SJ. 2003. Geoarchaeology of the Milfield Basin, northern England; towards an integrated archaeological prospection, research and management framework. *Archaeological Prospection* **9**: 71-91.

Payton, R. 1980. The soils of the Milfield Plain, Northumbrland. *North of England Soils Discussion Group Proceedings* **16**: 1-52.

Roering JJ, Mackey BH, Marshall JA, Sweeney KE, Deligne N, Booth AM, Handwerger AL, Cerovski-Darriau C. 2013. ‘You are HERE’: Connecting the dots with airborne lidar for geomorphic fieldwork. Geomorphology **200**: 172-183.

Smith MJ, Clarke CD. 2005. Methods of the visualisation of digital elevation models for landform mapping. *Earth Surface Processes and Landforms* **30**: 885-900.

Smith MJ. 2011. Digital mapping: Visualisation, interpretations and quantification of landforms. *Development in Earth Surface Processes* **15**: 225-251.

Teller JT, Leverington DW, Mann JD. 2002. Freshwater outbursts to the oceans from glacial Lake Agassiz and their role in climate change during the last deglaciation. *Quaternary Science Reviews* **21**: 871-887.

Van Den Eeckhaut M, Poesen J, Gullentops F, Vandekerckhove L, Hervás J. 2011. Regional mapping and characterisation of old landslides in hilly regions using LiDAR-based imagery in Southern Flanders. *Quaternary Research* **75**: 721-733.

Table 1

Event Sequence	**Surface Area (m^2)**	**Volume (m^3)**	**Volume change**	**Q (m^3/s)**	**Time (s)**	**Time (days)**
63m Lake Level	9.5×10^7	1.7×10^9	-	-	-	-
Phase 1 Breach (63m lake level)						
Accommodation space above gorge	4.5×10^6	2.5×10^7	-	3140 (1065)	7.8×10^3 2.3×10^4	0.09 (0.27)
Phase 1 erosion (downstream of breach)	3.5×10^6	3.0×10^7	-	3140 (1065)	9.5×10^3 2.8×10^4	0.11 (0.32)
Breach control:						
Lake fall 63-60m	8.5×10^7	1.3×10^9	3.6×10^8	3140 (1065)	1.3×10^5 (3.8×10^5)	1.5 (4.3)
Spillway control:						
Lake fall 60-55m	7.0×10^7	8.5×10^8	4.4×10^8	1000 (100)	4.5×10^5 (4.5×10^6)	5.2 (52.1)
Lake fall 55-50m	5.5×10^7	5.1×10^8	3.5×10^8	1000 (100)	3.4×10^5 (3.4×10^6)	3.9 (39.4)
Lake fall 50-45m	4.0×10^7	2.5×10^8	2.6×10^8	1000 (100)	2.6×10^5 (2.6×10^6)	3.0 (30.1)
Phase 2 Breach (ca. 45m lake level - possible still stand of unknown duration):						
Lake fall 45-40m	2.6×10^7	8.7×10^7	1.6×10^8	1000 (100)	1.6×10^5 (1.6×10^6)	1.9 (18.9)

Final lake drainage (40-31m)	0	0	8.7×10^7	1000 (100)	8.7×10^4 (8.7×10^5)	1.0 (10.1)
Event duration range						16-155

Table 2

	Eroded volume (m^3)	**Eroded area (m^2)**	**Estimated Duration (days)**	**Sediment Yield ($\times 10^6$ $t/km^2/yr$)**	**Mean rate of incision (m/day)**
Phase 1	2.3×10^7 (4.7×10^7) 2.3×10^7 (4.7×10^7)	3.5×10^6	13.6 13.6 126 126	392 798 42 86	0.37 0.04
Phase 2	8.2×10^6 (1.7×10^7) 8.2×10^6 (1.7×10^7)	1.4×10^6	2.9 2.9 29 29	1626 3309 162 331	2.87 0.29
Total erosion	3.1×10^7 (6.4×10^7)	3.5×10^6	16.5 155	355 (722) 37 (77)	0.81 (0.09)
Volume of eroded gorge material as a percentage of lake volume	1.9-3.8%				

Figure captions

Figure 1. Map of the study region showing the location of the Till gorge between the Milfield Plain and River Tweed. The Till gorge study reach is denoted by the extent of the 1m LiDAR coverage.

Figure 2. Greyscale raster image showing the spatial extent of the 1m and 2m LiDAR data and location of the cross-sections used in Figure 5. The Till gorge is divided into 100 m stations which are referred to in the text to locate the geomorphological features discussed, and in the figure captions to denote spatial location within the gorge. Place names referred to in the text are shown (CH = Castle Heaton).

Figure 3. LiDAR visualisations (1m resolution) at three locations in the Till gorge. Upper panels: Stations 2.7-3.4 km: a) Triangular Irregular Network (TIN) with hillshade effect - elevation greyscale produced at equal intervals (ca.3.6 m) with a range in the image of 11.4 m (light) to 64.2 m (dark); b) Slope digital terrain model (DTM). Middle panels: esker landform to the north of stations 7.0-8.6 km: c) TIN with hillshade effect - elevation greyscale produced at equal intervals (ca.3.6 m) with a range in the image of 20.6 m (dark) to 74.4 m (light); d) Slope DTM with transparent TIN overlay – same TIN as 3c) but, with hillshade effect removed. Lower panels: Stations 7.7-10.0 km e) hillshade with a 45° azimuth; and f) hillshade with a 225° azimuth.

Figure 4. Geomorphological map of the Till gorge study reach.

Figure 5. Cross-sections along the Till gorge demonstrating form and areal variability along the reach. Cross-sections are annotated with some of the key features and localities discussed in the text: e.g. Mill Hill drumlin and spillway and the Tiptoe eddy. Note the decreasing cross sectional areas of the uppermost cross sections at 9.73 km and 10.11 km.

Figure 6. Sedimentary exposure at station 5.0 km located against the upstream side of the dyke. Note the imbricated rip-up boulders of the local Carboniferous sandstone (Ballagan Formation) and Late Carboniferous quartz microgabbro dyke material, within a matrix of fluvially sorted pea-size gravels and sands.

Figure 7. Till valley long-profile summarising the main geomorphic evidence from the Till gorge and Milfield Plain. The 1.5 km long contemporary Crookham meander has been removed to demonstrate straight line distance down-valley from the Milfield Plain to the Till gorge. The dashed lines on the gorge rim show locations where gorge orientation and morphology precludes defining a clear gorge lip. Note the shallow slope between the two T1 terrace surfaces upstream of Mill Hill reflecting backflooding prior to Phase 2 incision.

Figure 8. Triangular Irregular Networks (TINs) of the Till gorge with annotated flow circulation during the GLOF: a) the lower reach (stations 0.8-6.1 km) and b) the upper reach (stations 4.5-10.0 km). Note the elevation shading is different between the two TINs and has been selected to highlight the key morphology related to flow pathways as the event proceeded.

Figure 9. a) Mean depths along the Till gorge demonstrating incision history. The phase 1 and 2 depths are constrained by the geomorphological evidence in the gorge. Note that the main phase 1 incision occurs at the breach site (station 7.6 km) with relatively limited incision downstream as the flow spilled across the landscape and was backflooded by Mill Hill. Greater incision occurred during Phase 2 (breach site at station 2.2 km) as flow was more concentrated in the gorge. Also note the mean depth of both phases decreasing upstream reflecting the pattern of knickpoint retreat. b) Plot of volume of water versus sediment released during the outburst flood (x). The linear trend is the bootstrap curve for observed outburst events compiled by Korup (2012).

Figure 10. Slope DTMs from the Till gorge upper reach (stations 9.3-10.1 km): a) 1m LiDAR; b) 2m LiDAR; c) resampled 5m; and d) resampled 10m. Darker grey scale indicates steeper gradient and vice versa.

Figure 11. Maps of the Milfield basin. a) 63m lake extent of Palaeolake Milfield and at the 50m and 40m intermediary stages as lake level drops. Note the emerging Glen fan surface and the islands exposed once 40m elevation is reached. b) 1m LiDAR derived TIN showing abandoned palaeochannels, created by knickpoint retreat, either side of the contemporary river and Holocene meander belt. It is likely that the Etal-Heatherslaw bend is an artefact of backflooding and eddying as lake waters approached the breach site.

Figure 12. a) Proposed ice limits according to mapped (Milfield and Bowmont) and hypothesised (Leet) palaeolakes, kettle moraine topography and incised drainage pathways (white lines). b) 1m LiDAR derived TIN showing a hypothesised ice-dammed lake denoting an ice margin. The incised channel is currently dry and is aligned up-valley. c) LiDAR slope map (darkening grey scale indicates steeper gradients) showing the key geomorphology of Palaeolake Bowmont: the breached moraine dam, shoreline and delta-fans.

Figure 13 Slope DTM (1m LiDAR) of the Glen valley showing the palaeochannels and scarp slopes of the delta fan surface. Solid arrows indicate flow pathways once the GLOF has started. As the lake level drops eddy circulation (broken arrows) is hypothesised to occur created by flow pathways from the Glen Valley and the morphology of the emerging land surface. The morphology of the scarp slopes indicate scouring by eddy flow circulation whilst to the east of the fan slumped material is evident.

Table Captions

Table 1. Event sequence and duration quantified from spatial data and discharge (Q) estimates. The dam breach discharges were calculated using Costa and Schuster's (1988) empirical equation $Q = 3.8(DV)^{0.61}$ where D is the dam height (m) and v is the lake volume ($m^3 \times 10^6$). The spillway control flow was calculated based on the experimental equation (Eq. 14-9 in Chow, 1958, p362) for flow over a sharp crested weir: $Q = CLH^{1.5}$ where L is the effective length of the weir crest; H is the head above the crest (excluding velocity head); and C is the discharge coefficient defined by the equation $C = 3.27 + 0.40(H/h)$ where h is the height of the weir. As the effective height of the weir was unknown we modelled C values for the range of usual H/h values (<10), reported by Chow (1958). The final values were recorded as orders of magnitude (10^2-10^3 m^3/s) due to the uncertainties involved.

Table 2. Quantified erosion rates and volumes based on upper and lower calculations of eroded volumes and event duration.

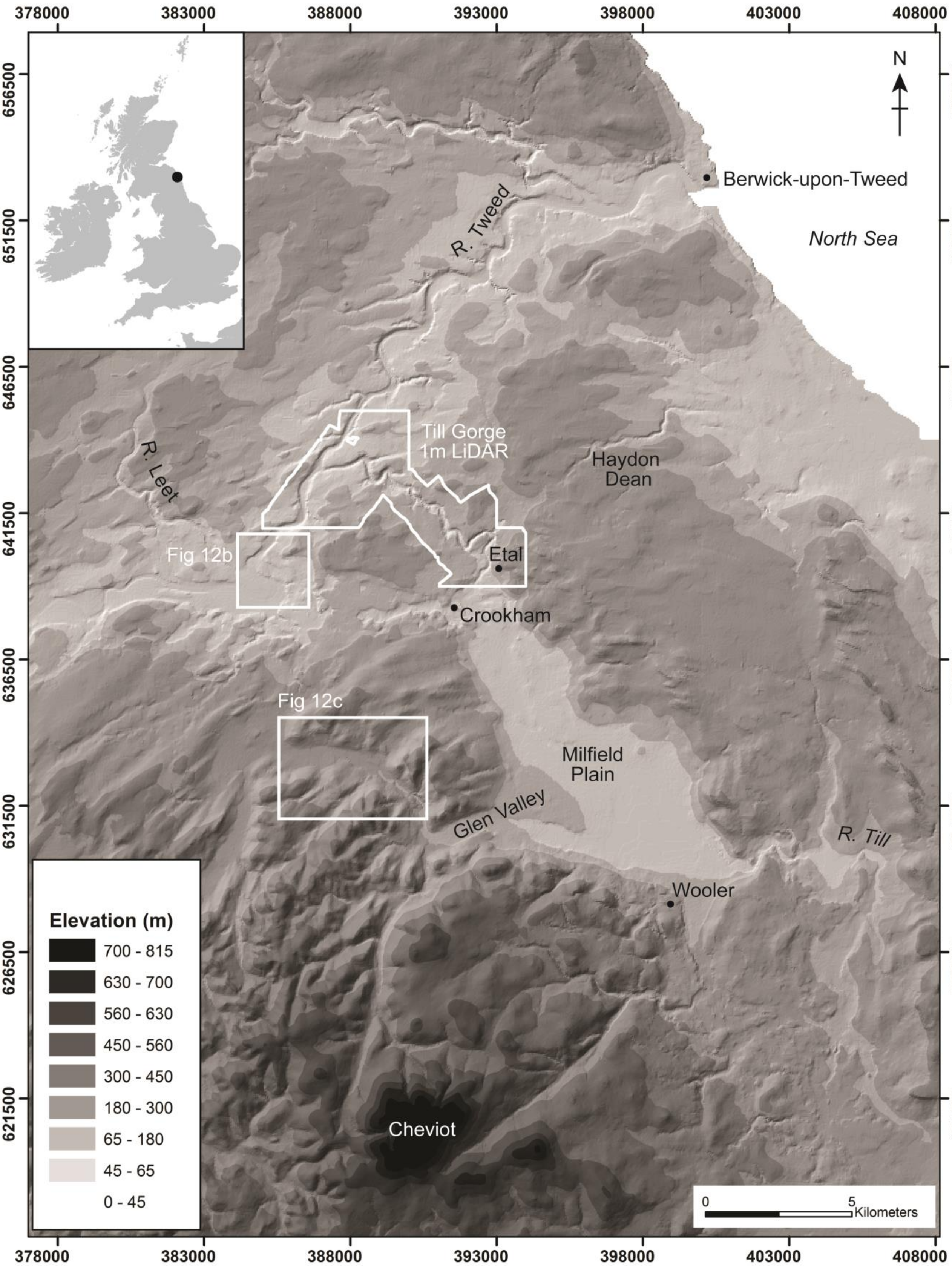

378000
383000
388000
393000
398000
403000
408000
656500
651500
646500
641500
636500
631500
626500
621500
N
Berwick-upon-Tweed
North Sea
R. Tweed
R. Leet
Till Gorge
1m LiDAR
Haydon
Dean
Fig 12b
Etal
Crookham
Fig 12c
Milfield
Plain
Glen Valley
R. Till
Wooler
Elevation (m)
700 - 815
630 - 700
560 - 630
450 - 560
300 - 450
180 - 300
65 - 180
45 - 65
0 - 45
Cheviot
0
5
Kilometers

Fig 1

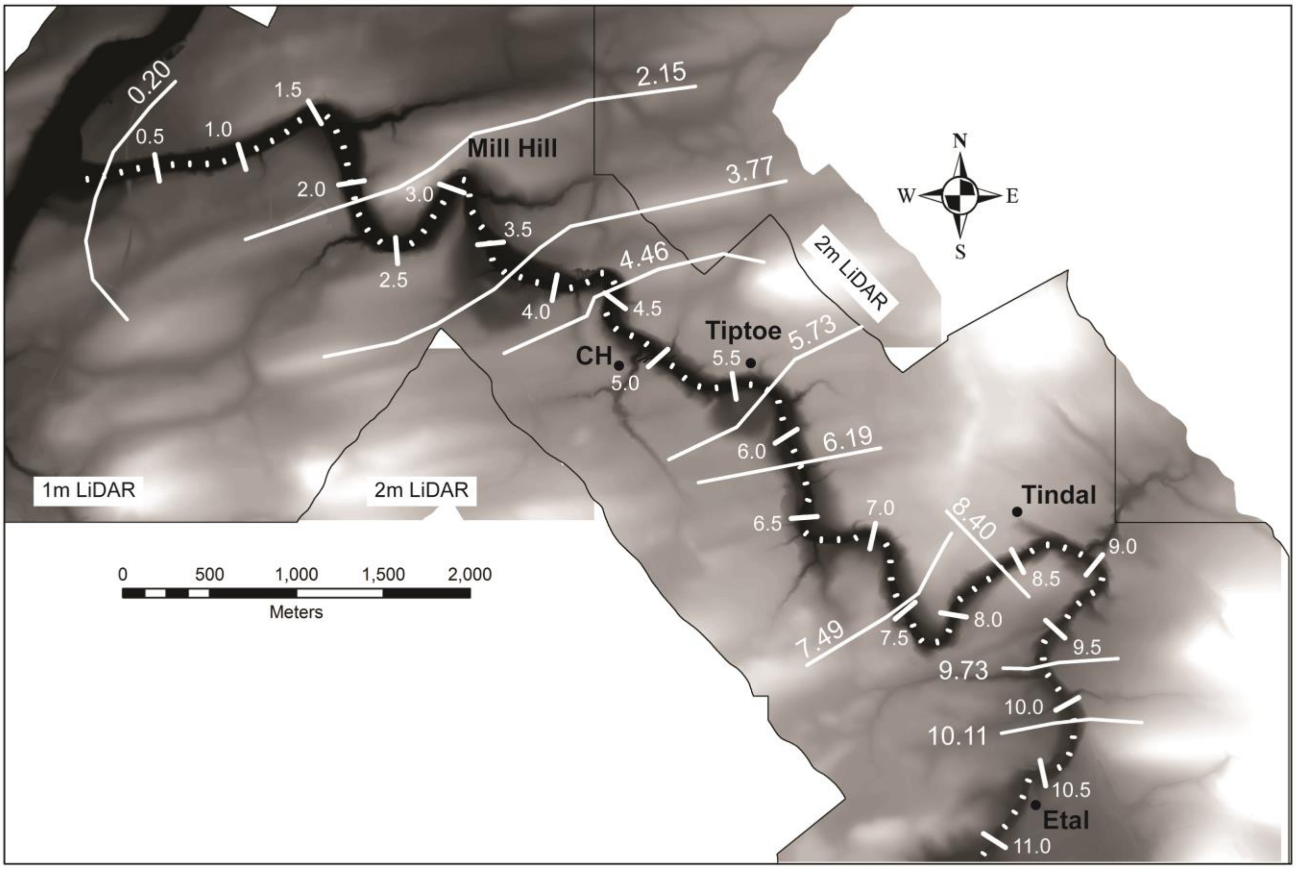
0.20
0.5
1.0
1.5
2.15
Mill Hill
2.0
3.0
3.77
3.5
2.5
4.46
4.0
4.5
2m LiDAR
Tiptoe
5.73
CH
5.5
5.0
6.0
6.19
1m LiDAR
2m LiDAR
Tindal
8.40
7.0
6.5
9.0
8.5
8.0
7.49
7.5
9.5
9.73
10.0
10.11
10.5
Etal
11.0
0
500
1,000
1,500
2,000
Meters
N
W
E
S

Fig. 2

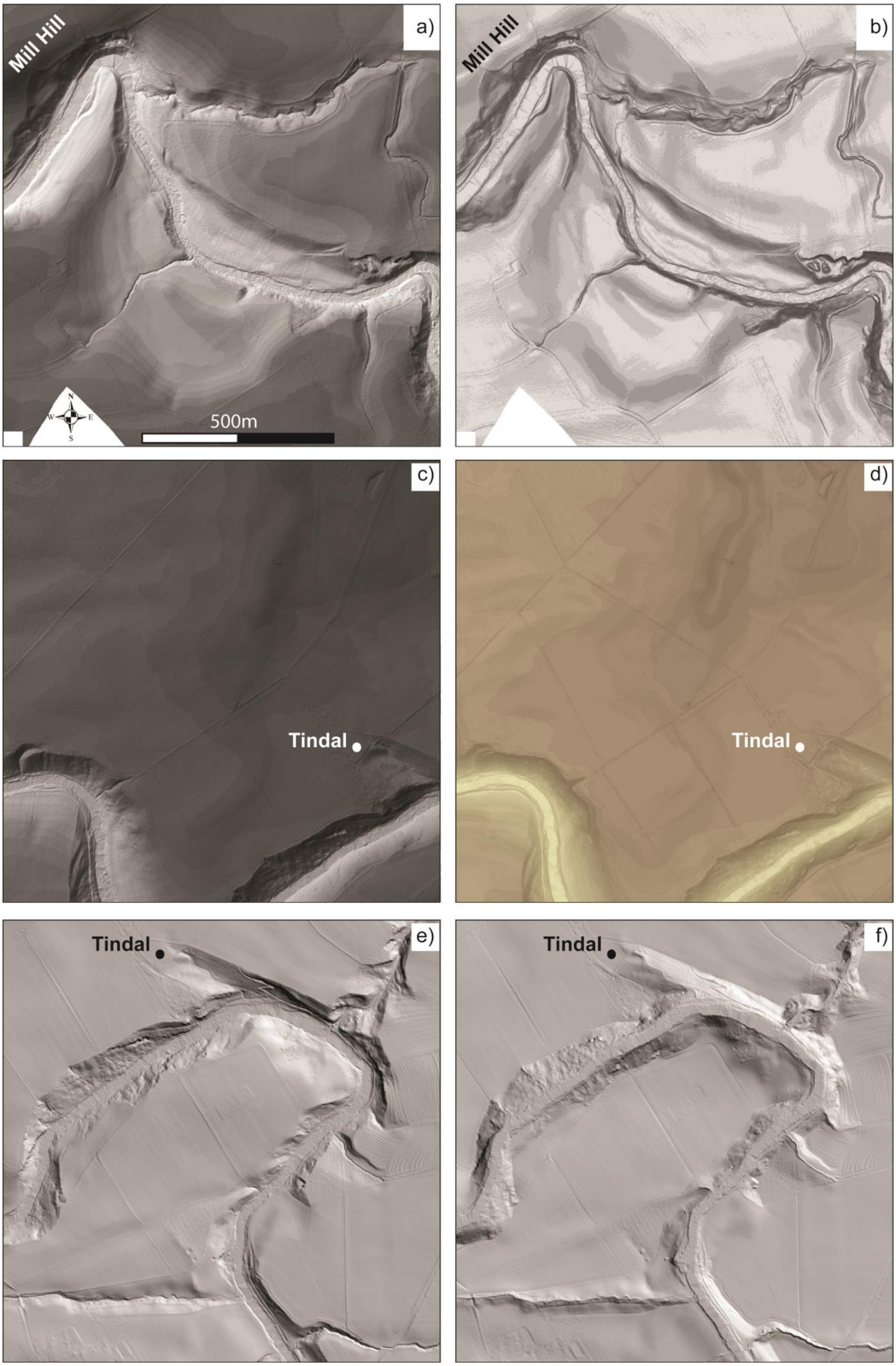

Mill Hill
a)
500m
Mill Hill
b)
c)
Tindal
d)
Tindal
e)
Tindal
f)
Tindal

Fig 3

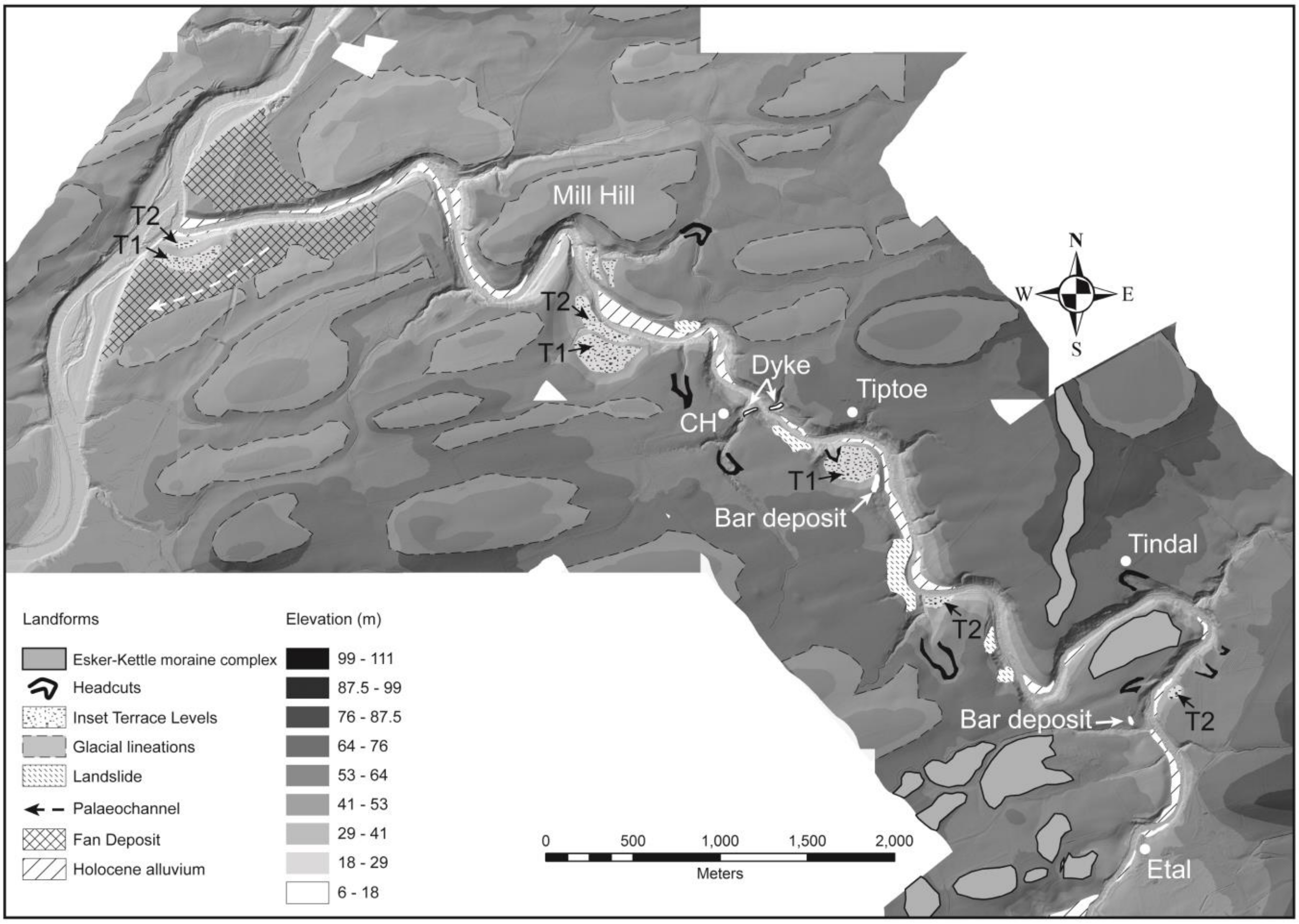
Mill Hill
T2
T1
T2
T1
Dyke
Tiptoe
CH
T1
Bar deposit
Tindal
T2
Bar deposit
T2
Etal
N
W
E
S
Landforms
Esker-Kettle moraine complex
Headcuts
Inset Terrace Levels
Glacial lineations
Landslide
Palaeochannel
Fan Deposit
Holocene alluvium
Elevation (m)
99 - 111
87.5 - 99
76 - 87.5
64 - 76
53 - 64
41 - 53
29 - 41
18 - 29
6 - 18
0
500
1,000
1,500
2,000
Meters

Fig. 4

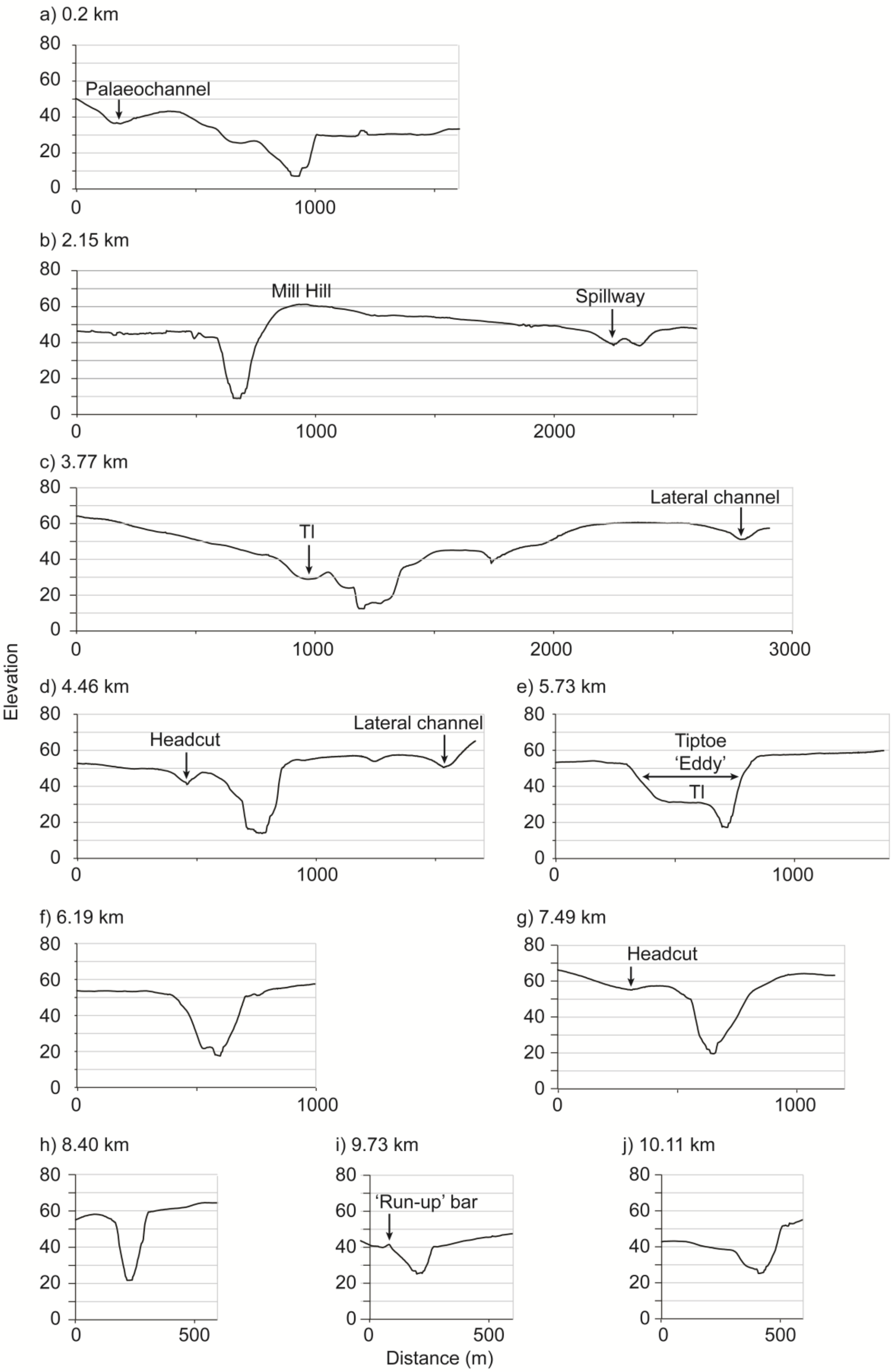
a) 0.2 km
Palaeochannel
b) 2.15 km
Mill Hill
Spillway
c) 3.77 km
TI
Lateral channel
Elevation
d) 4.46 km
Headcut
Lateral channel
e) 5.73 km
Tiptoe
'Eddy'
TI
f) 6.19 km
g) 7.49 km
Headcut
h) 8.40 km
i) 9.73 km
'Run-up' bar
j) 10.11 km
Distance (m)
0
20
40
60
80
500
1000
2000
3000

Fig. 5

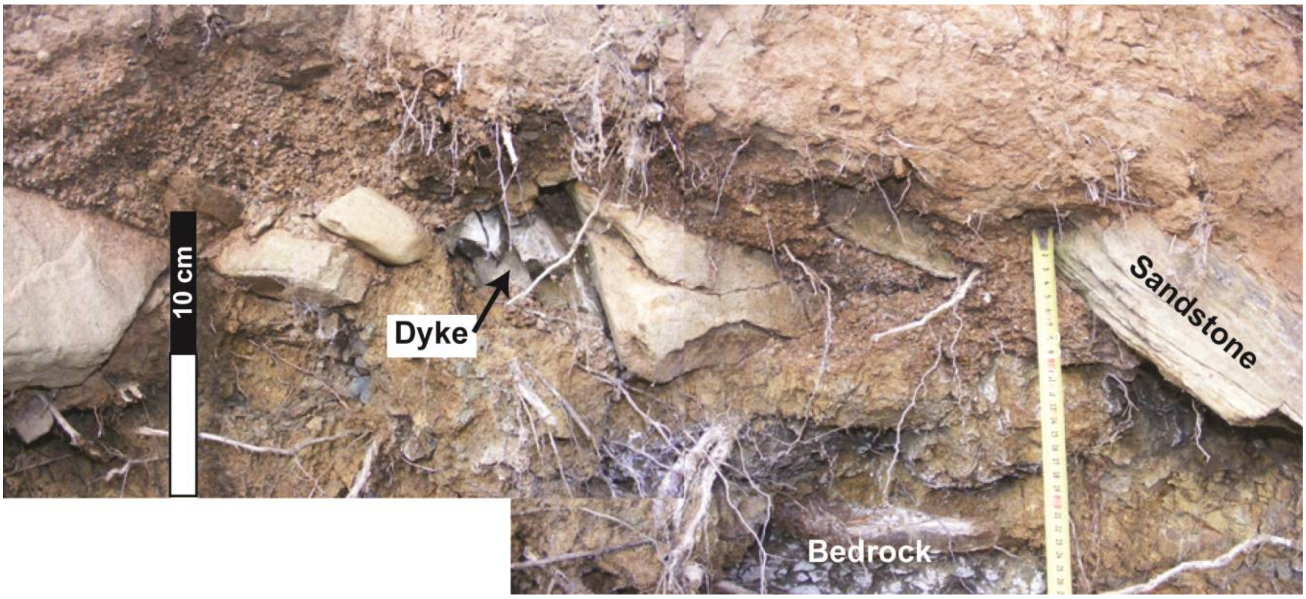

Fig. 6

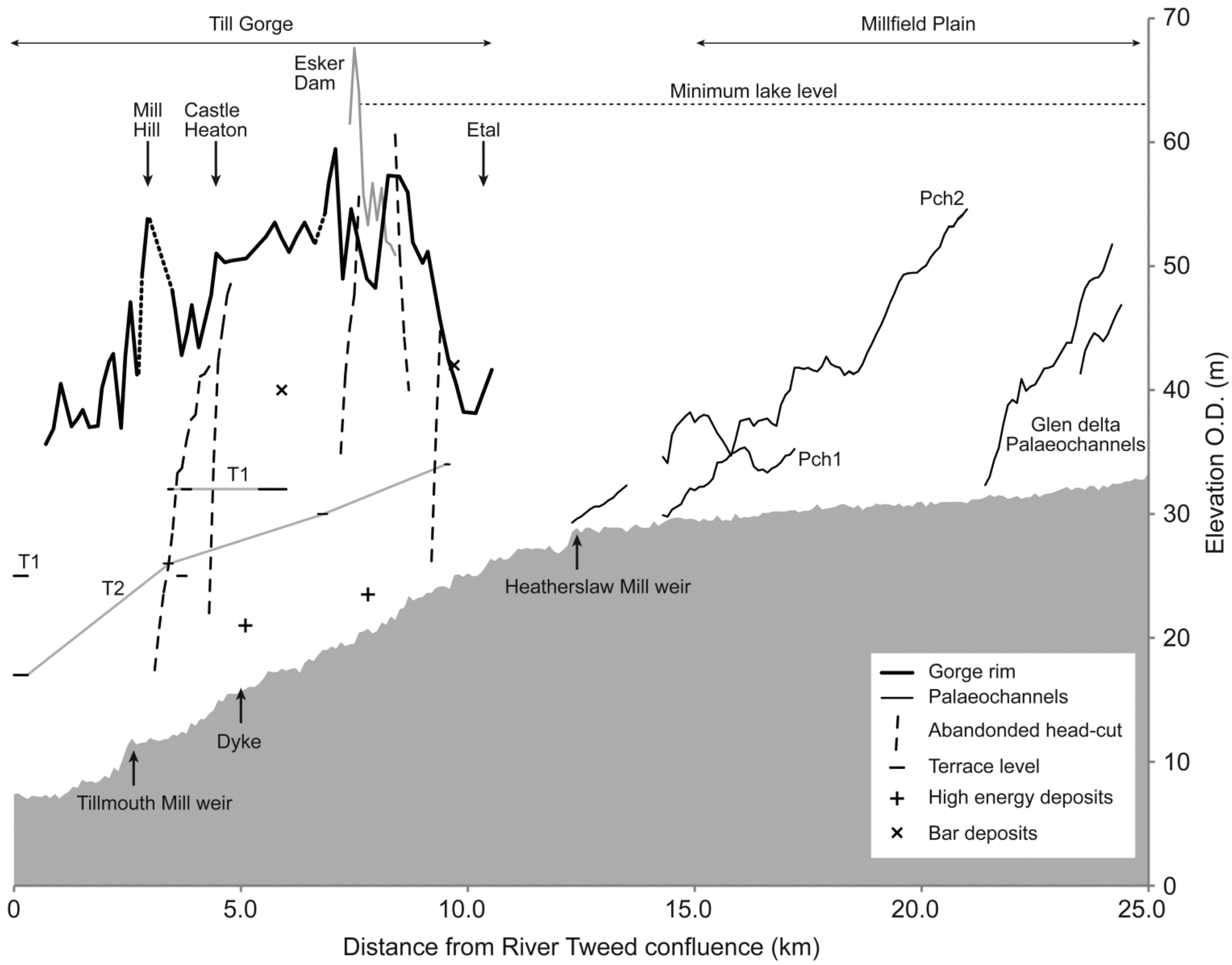

Till Gorge
Millfield Plain
Esker
Dam
Minimum lake level
Mill
Hill
Castle
Heaton
Etal
Pch2
Pch1
Glen delta
Palaeochannels
T1
T1
T2
Heatherslaw Mill weir
Dyke
Tillmouth Mill weir
Gorge rim
Palaeochannels
Abandonded head-cut
Terrace level
High energy deposits
Bar deposits
Elevation O.D. (m)
Distance from River Tweed confluence (km)
0
5.0
10.0
15.0
20.0
25.0
10
20
30
40
50
60
70

Fig. 7

909

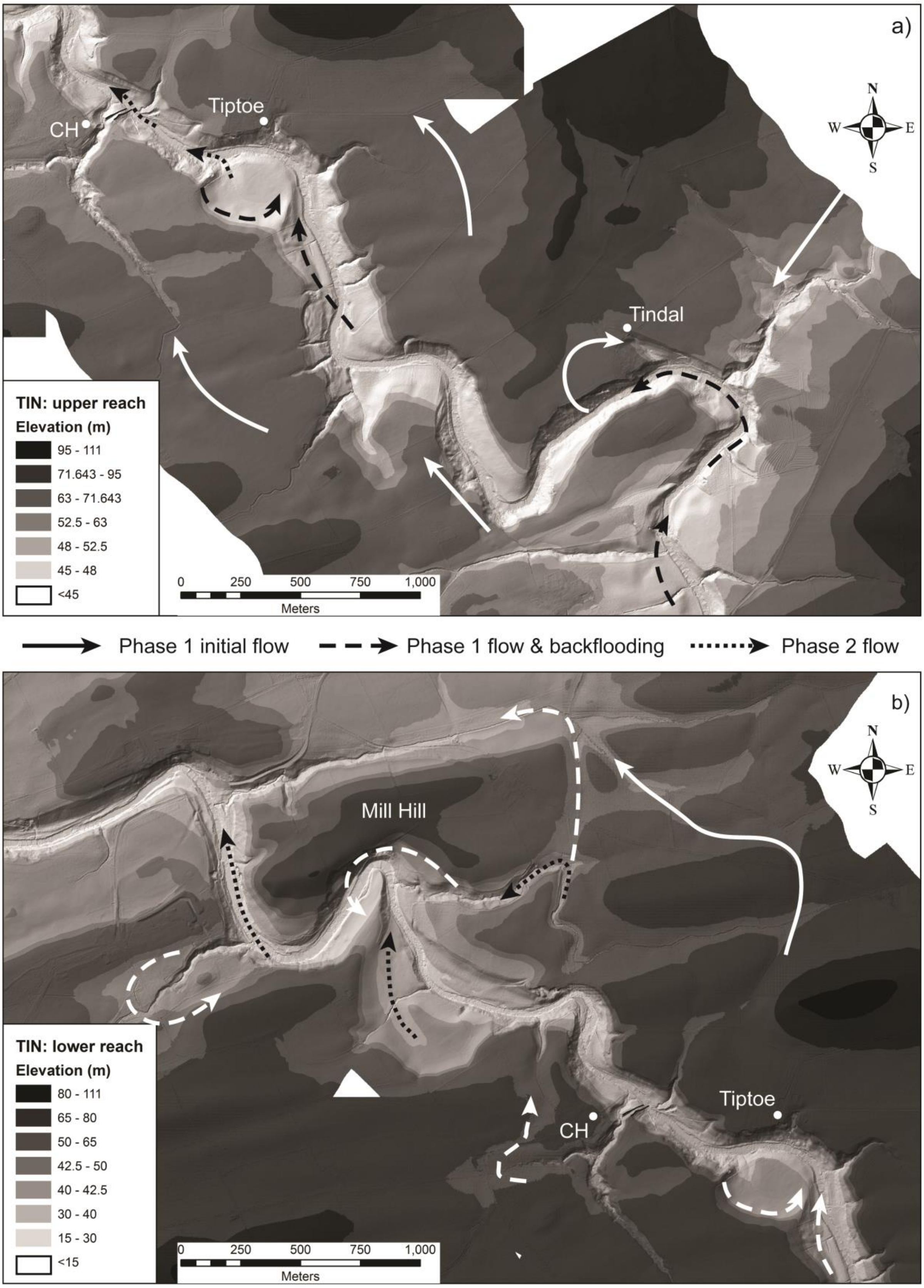
a)
Tiptoe
CH
Tindal
TIN: upper reach
Elevation (m)
95 - 111
71.643 - 95
63 - 71.643
52.5 - 63
48 - 52.5
45 - 48
<45
0 250 500 750 1,000
Meters
N
W
E
S
Phase 1 initial flow
Phase 1 flow & backflooding
Phase 2 flow
b)
Mill Hill
CH
Tiptoe
TIN: lower reach
Elevation (m)
80 - 111
65 - 80
50 - 65
42.5 - 50
40 - 42.5
30 - 40
15 - 30
<15
0 250 500 750 1,000
Meters

910 Fig. 8

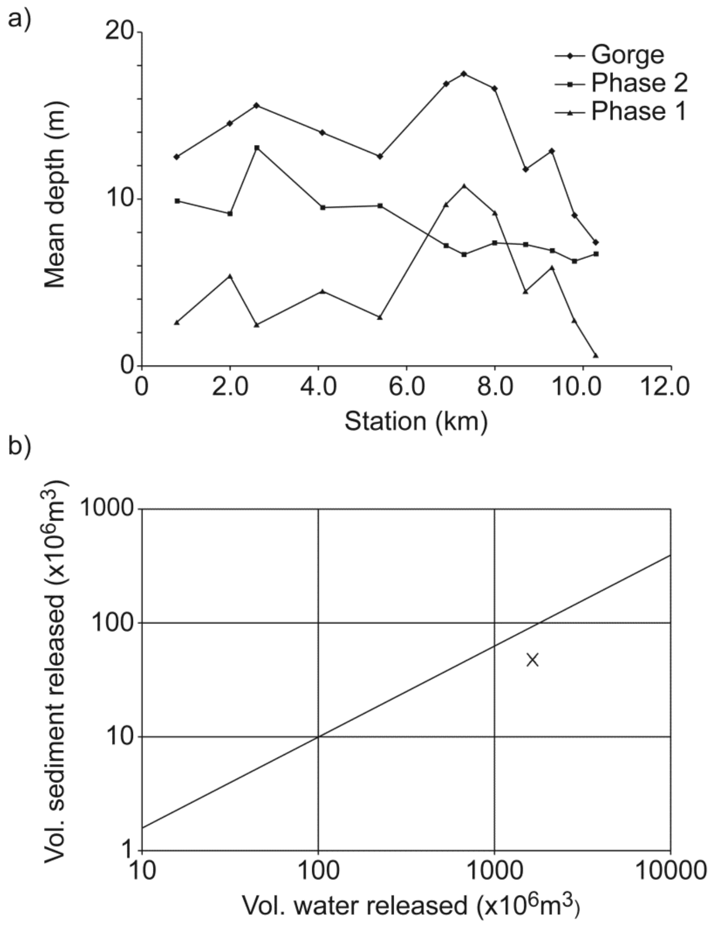
a)
Gorge
Phase 2
Phase 1
Mean depth (m)
Station (km)
0
10
20
2.0
4.0
6.0
8.0
10.0
12.0
b)
Vol. sediment released (x10^6m^3)
Vol. water released (x10^6m^3)
1
10
100
1000
10000

Fig. 9

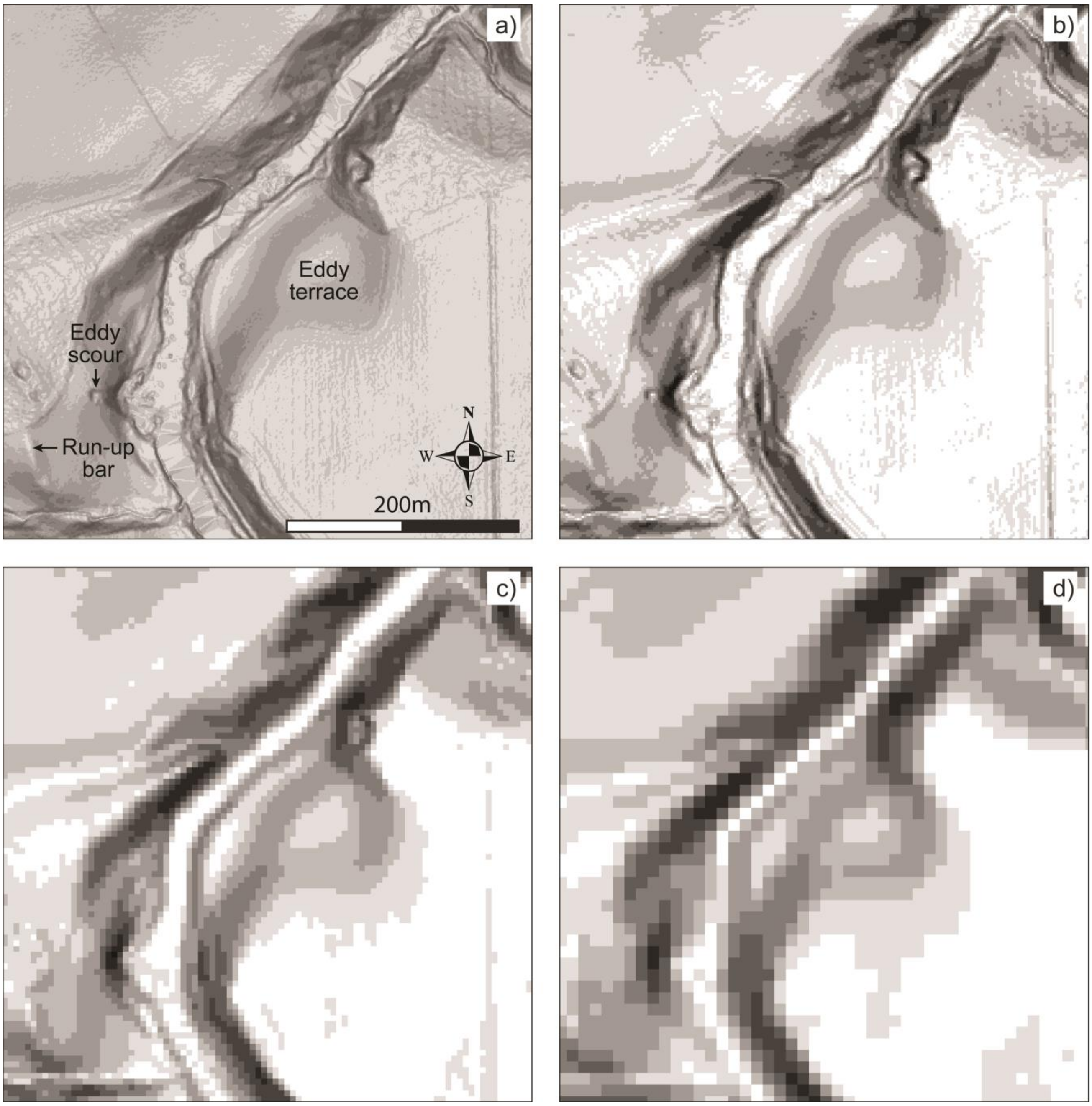

Fig.10

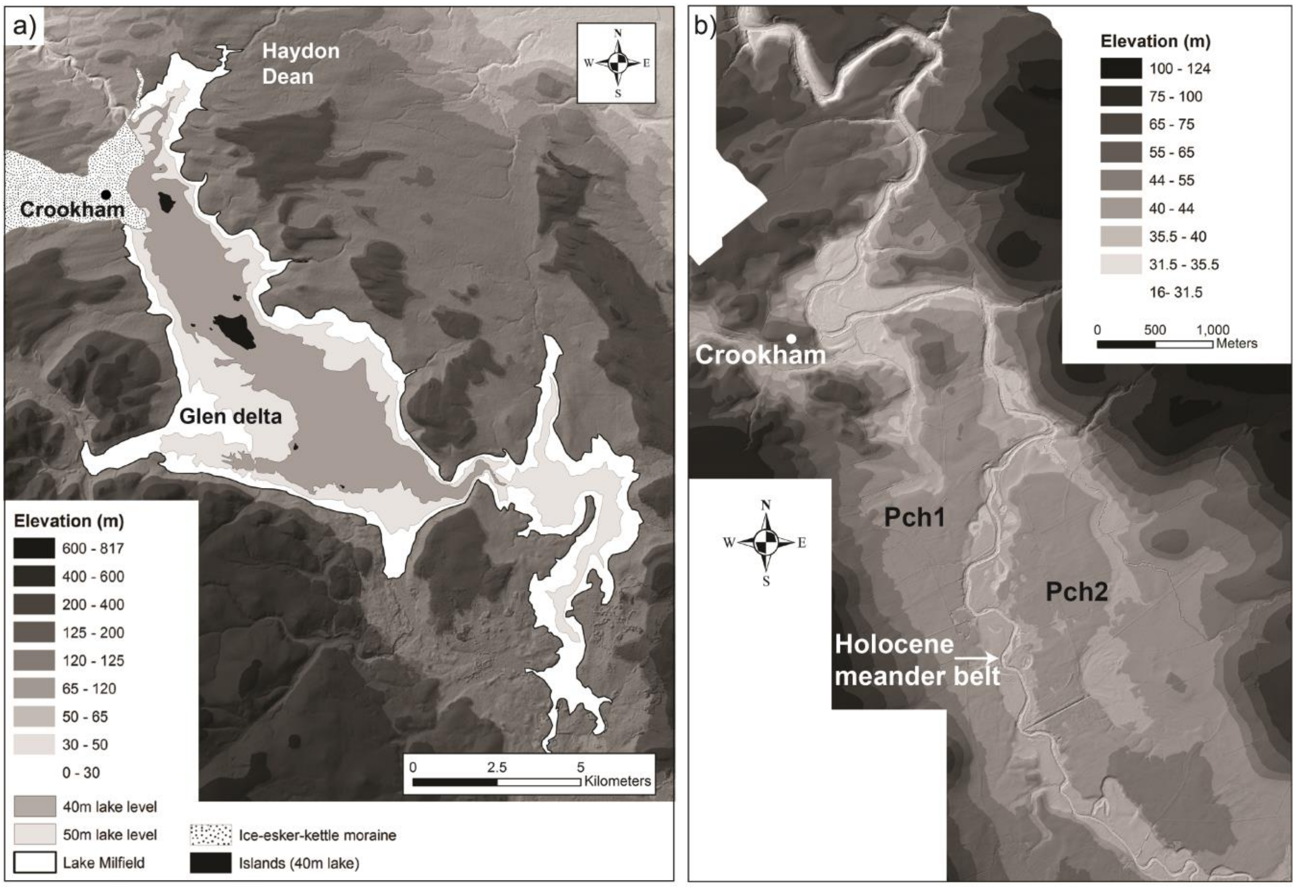
a)
Haydon Dean
Crookham
Glen delta
N
W
E
S
Elevation (m)
600 - 817
400 - 600
200 - 400
125 - 200
120 - 125
65 - 120
50 - 65
30 - 50
0 - 30
0
2.5
5
Kilometers
40m lake level
50m lake level
Lake Milfield
Ice-esker-kettle moraine
Islands (40m lake)
b)
Elevation (m)
100 - 124
75 - 100
65 - 75
55 - 65
44 - 55
40 - 44
35.5 - 40
31.5 - 35.5
16- 31.5
0
500
1,000
Meters
Crookham
Pch1
Pch2
Holocene meander belt

Fig. 11

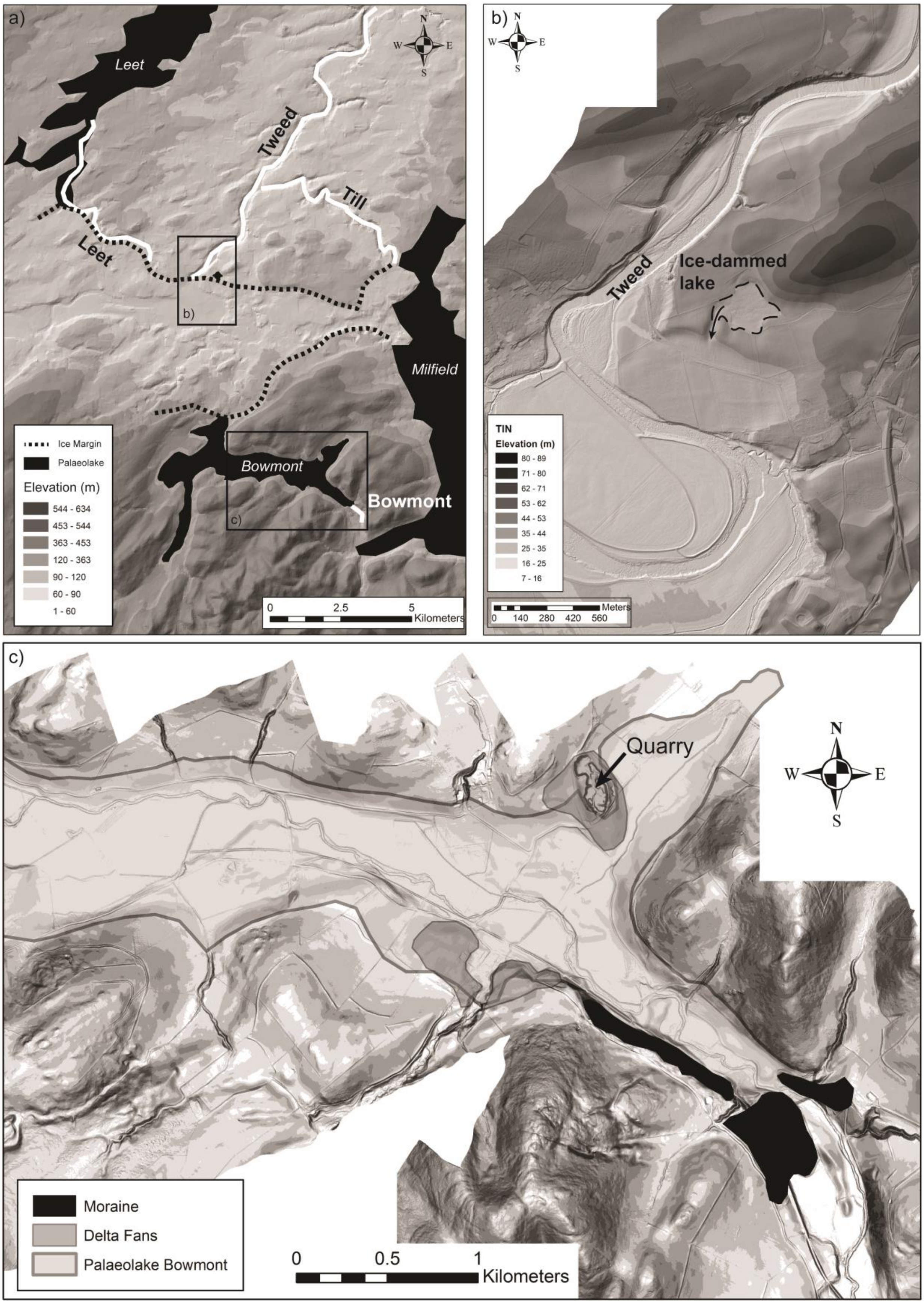
a)
Leet
Tweed
Till
Leet
b)
Milfield
Bowmont
Bowmont
c)
Ice Margin
Palaeolake
Elevation (m)
544 - 634
453 - 544
363 - 453
120 - 363
90 - 120
60 - 90
1 - 60
0 2.5 5 Kilometers
b)
Tweed
Ice-dammed lake
TIN
Elevation (m)
80 - 89
71 - 80
62 - 71
53 - 62
44 - 53
35 - 44
25 - 35
16 - 25
7 - 16
0 140 280 420 560 Meters
c)
Quarry
N
W
E
S
Moraine
Delta Fans
Palaeolake Bowmont
0 0.5 1 Kilometers

Fig. 12

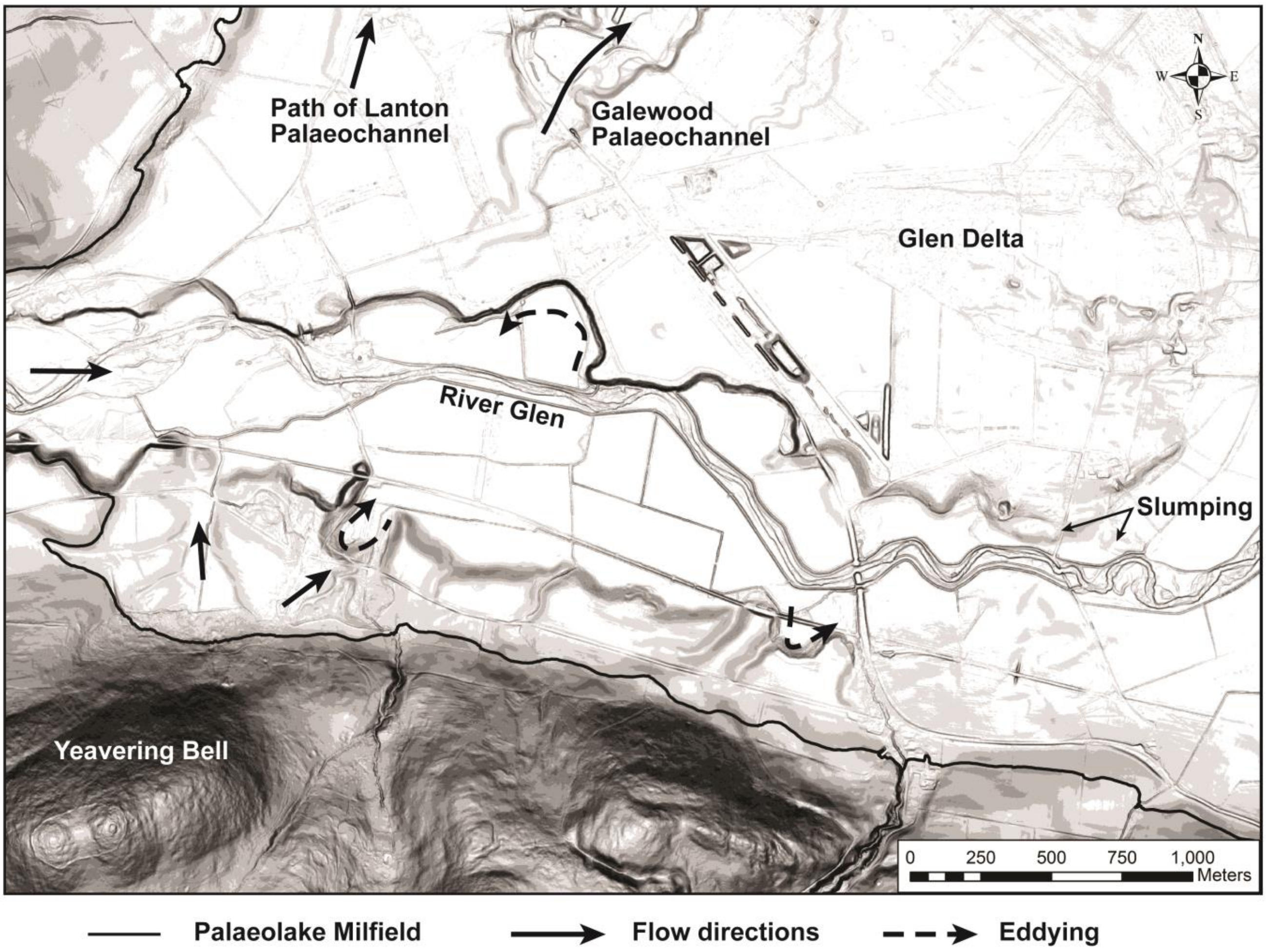
Path of Lanton
Palaeochannel
Galewood
Palaeochannel
Glen Delta
River Glen
Slumping
Yeavering Bell
N
W
E
S
0
250
500
750
1,000
Meters
Palaeolake Milfield
Flow directions
Eddying

Fig. 13